nature methods

BRIEF COMMUNICATION

https://doi.org/10.1038/s41592-018-0294-6

A genetically encoded near-infrared fluorescent calcium ion indicator

Yong Qian[1,12], Kiryl D. Piatkevich[2,12], Benedict Mc Larney[3,4,12], Ahmed S. Abdelfattah[5], Sohum Mehta[6], Mitchell H. Murdock[2], Sven Gottschalk[3], Rosana S. Molina[7], Wei Zhang[1], Yingche Chen[1], Jiahui Wu[1], Mikhail Drobizhev[7], Thomas E. Hughes[7], Jin Zhang[6], Eric R. Schreiter[5], Shy Shoham[8], Daniel Razansky[3,4,9,10], Edward S. Boyden[2] and Robert E. Campbell[1,11]*

We report an intensiometric, near-infrared fluorescent, genetically encoded calcium ion (Ca^{2+}) indicator (GECI) with excitation and emission maxima at 678 and 704 nm, respectively. This GECI, designated NIR-GECO1, enables imaging of Ca^{2+} transients in cultured mammalian cells and brain tissue with sensitivity comparable to that of currently available visible-wavelength GECIs. We demonstrate that NIR-GECO1 opens up new vistas for multicolor Ca^{2+} imaging in combination with other optogenetic indicators and actuators.

GECIs are often used together with optogenetic actuators for simultaneous recording and control of biological processes with high spatiotemporal resolution. However, substantial spectral overlap among currently available GECIs, optogenetic actuators and other genetically encoded indicators limits the possibilities for multiplexing. Most genetically encoded fluorophores fall into two classes: visibly fluorescent β-barrel fluorescent proteins that are homologs of the *Aequorea* green fluorescent protein[1], and far-red to near-infrared (NIR) fluorescent biliverdin-binding fluorescent proteins (BV-FPs) derived from bacteriophytochromes (BphPs)[2] or other biliverdin-binding proteins[3]. Fluorescent proteins have emission peaks in the visible range (~450–670 nm), and BV-FPs have emission peaks in the NIR range (~670–720 nm)[4]. While many GECIs and other indicators have been engineered from fluorescent proteins, examples of BV-FP-based indicators are limited. Examples include BV-FPs as donors and acceptors in fluorescence resonance energy transfer (FRET)-based indicators, and the use of split BV-FPs in protein complementation assays[5].

To expand the range of GECI colors into the NIR range, we have engineered an intensiometric GECI on the basis of the monomeric BV-FP, mIFP[6]. We pursued a design with a Ca^{2+}-binding domain (calmodulin (CaM)-RS20), inserted into mIFP such that Ca^{2+} binding would modulate the biliverdin chromophore environment and fluorescence intensity (Supplementary Note 1). We chose four potential insertion sites (between residues 9/10, 57/58, 138/139 and 170/176) based on inspection of the X-ray crystal structure of *Deinococcus radiodurans* BphP (PDB ID: 2O9B)[7], which has 35% sequence identity with mIFP[6]. Only the replacement of residues 171–175 with CaM-RS20 yielded a protein with a Ca^{2+}-dependent change in fluorescence in vitro (a twofold decrease) (Fig. 1a,b and Supplementary Fig. 1). To improve the indicator properties, we systematically optimized the insertion site (leading to deletion of mIFP residues 176 and 177) and the N- and C-terminal linkers (ultimately the sequences GAL and RRHD, respectively) connecting CaM-RS20 to mIFP.

To facilitate iterative rounds of improvement on the basis of fluorescence screening of randomly mutated variants in bacterial colonies followed by functional tests in mammalian cells, we created a vector (*pcDuEx2*) for expression in both *Escherichia coli* and mammalian cells (Supplementary Fig. 2a). Following 12 rounds of library expression and screening (Supplementary Figs. 2b and 3), we designated our best variant as NIR genetically encoded Ca^{2+} indicator for optical imaging (NIR-GECO1; Supplementary Figs. 2c and 4). A parallel effort to engineer a GECI from the smURFP[3] BV-FP was not successful (Supplementary Fig. 5). NIR-GECO1 has absorbance and emission peaks at 678 and 704 nm, respectively, and undergoes a 90% decrease in fluorescence intensity upon binding Ca^{2+} (K_d = 215 nm) (Fig. 1c–e and Supplementary Fig. 6). The fluorescence change and K_d are comparable to those of GCaMP3 (F_{max}/F_{min} = 13.6; K_d = 405 nm), which was the first broadly useful single-fluorescent-protein-based GECI[8]. Key differences include the opposite directions of the responses to Ca^{2+} and NIR-GECO1's lower Hill coefficient (n = 1.03). As an inverse response indicator, NIR-GECO1 is in its more brightly fluorescent form in resting cells (low Ca^{2+}), and is therefore more susceptible to photobleaching under continuous illumination. In addition, excitation of resting cells above and below the imaging plane will contribute to an increased background signal. As expected when comparing an FP to a BV-FP, the Ca^{2+}-bound state of GCaMP3 is approximately sixfold brighter than the Ca^{2+}-free state of NIR-GECO1 (Supplementary Table 1)[8].

To evaluate the performance of NIR-GECO1 in cultured neurons, we compared intracellular fluorescence brightness and photostability to those of the spectrally similar BV-FPs, iRFP682[9] and miRFP[10] (Supplementary Table 1). All three BV-FPs distributed evenly within the cytosol, dendrites and nucleus of neurons, with no apparent puncta or localized accumulations (Fig. 1f). NIR-GECO1 baseline intracellular brightness was similar to that of miRFP and

[1]Department of Chemistry, University of Alberta, Edmonton, Alberta, Canada. [2]Media Lab and McGovern Institute for Brain Research, MIT, Cambridge, MA, USA. [3]Institute for Biological and Medical Imaging, Helmholtz Center Munich, Neuherberg, Germany. [4]Faculty of Medicine, Technical University of Munich, Munich, Germany. [5]Janelia Research Campus, Howard Hughes Medical Institute, Ashburn, VA, USA. [6]Department of Pharmacology, University of California San Diego, La Jolla, CA, USA. [7]Department of Cell Biology and Neuroscience, Montana State University, Bozeman, MT, USA. [8]Departments of Ophthalmology and of Neuroscience and Physiology, New York University Langone Health, New York City, NY, USA. [9]Faculty of Medicine and Institute of Pharmacology and Toxicology, University of Zurich, Zurich, Switzerland. [10]Department of Information Technology and Electrical Engineering and Institute for Biomedical Engineering, ETH Zurich, Zurich, Switzerland. [11]Department of Chemistry, Graduate School of Science, The University of Tokyo, Tokyo, Japan. [12]These authors contributed equally: Yong Qian, Kiryl D. Piatkevich, Benedict Mc Larney. *e-mail: robert.e.campbell@ualberta.ca

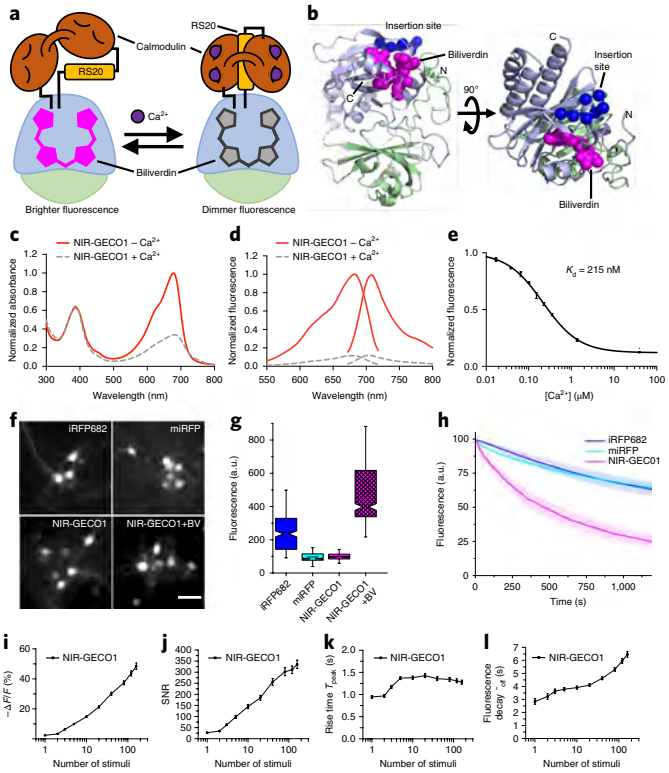

Fig. 1 | Structure and characterization of NIR-GECO1. a, Schematic representation of NIR-GECO1 and its mechanism of response to Ca^{2+}. The PAS domain is colored light green, and the biliverdin-binding GAF domain is colored light blue. RS20 is the CaM-binding peptide of smooth muscle myosin light chain kinase. **b**, Orthogonal views of the structure of *Dr*BphP (PDB 2O9B)[7], a close homolog of mIFP. The PAS and GAF domains are colored as in **a**, biliverdin is shown as magenta spheres, and the Cα atoms of the seven residues that were replaced with CaM-RS20 are shown as blue spheres. **c**, Absorbance spectra in the presence (39 μM) and absence of Ca^{2+}. **d**, Fluorescence excitation and emission spectra in the presence (39 μM) and absence of Ca^{2+}. **e**, Fluorescence of NIR-GECO1 as a function of Ca^{2+} concentration. Center values are the mean, and error bars are s.d. $n=3$ independent experiments. **f**, Representative wide-field fluorescence images (631/28 nm excitation (Ex) at 38 mW mm^{-2} and 664LP emission (Em)) of mouse neurons expressing iRFP682, miRFP, NIR-GECO1 and NIR-GECO1 supplemented with exogenous biliverdin (25 μM) ($n=263$, 326, 367 and 473 neurons for iRFP682, miRFP, NIR-GECO1 and NIR-GECO1 + biliverdin, respectively, from two cultures). The dynamic ranges of these images have been normalized to facilitate visual comparison of protein localization. Fluorescence brightness quantification provided in **g**. Scale bar, 50 μm. **g**, Relative fluorescence intensity for neurons shown in **f** (BV, biliverdin). Box plots with notches are used. The narrow part of notch is the median; the top and bottom of the notch denote the 95% confidence interval of the median; the horizontal line is the mean; the top and bottom horizontal lines are the 25th and 75th percentiles for the data; and the whiskers extend 1×1.5 the interquartile range from the 25th and 75th percentiles. **h**, Photobleaching curves for iRFP682, miRFP and NIR-GECO1 ($n=84$, 69 and 88 neurons, respectively, from two cultures; 631/28 nm Ex at 38 mW mm^{-2}; solid lines represent mean value, shaded areas represent s.d.). **i**–**l**, NIR-GECO1 response amplitude (**i**), signal-to-noise ratio (SNR) (**j**), rise time (actually a fluorescence decrease) for Ca^{2+} binding (**k**) and decay time (actually a fluorescence increase) for Ca^{2+} dissociation (**l**), as a function of the number of field stimulation-induced action potentials. Center values are the mean, and error bars are s.e.m. $n=55$ neurons.

2.5-fold lower than that of iRFP682 (Fig. 1g). Administration of 25 μM exogenous biliverdin for 3 h resulted in an approximately fivefold increase in the NIR-GECO1 baseline fluorescence (Fig. 1g), indicating that ~80% of NIR-GECO1 was not bound to biliverdin. The addition of biliverdin also resulted in a slight increase in the mean value of the NIR-GECO1 fluorescence changes during spontaneous activity (16 ± 6% versus 20 ± 8% $-\Delta F/F_0$ for NIR-GECO1 and NIR-GECO1 + biliverdin, respectively; mean ± s.d. throughout; Supplementary Fig. 7a,b). This biliverdin-free fraction is not fluorescent but presumably participates in contra-productive Ca^{2+} buffering. Coexpression of heme-oxygenase 1 (HO1) with NIR-GECO1[6] resulted in only a 1.4-fold enhancement of fluorescence intensity (Supplementary Fig. 7c,d). Under continuous wide-field illumination at 38 mW mm^{-2} (about two to four times higher than typically used for NIR-GECO1 imaging), the photobleaching rate of NIR-GECO1 was approximately fourfold higher than those of miRFP and iRFP682 (Fig. 1h and Supplementary Table 1).

To characterize the fluorescence response of NIR-GECO1 to electric field stimulation-evoked action potentials, we delivered field stimuli (50 V, 83 Hz, 1 ms) in trains of 1, 2, 3, 5, 10, 20, 40, 80, 120 and 160 to transfected neurons (Supplementary Fig. 8a). The resulting fluorescence changes, recorded from cell bodies, revealed that $-\Delta F/F_0$, SNR, rise time and decay time all increased with the number of stimuli (Fig. 1i–l). Relative to GCaMP3, NIR-GECO1 has similar $-\Delta F/F_{min}$ for 1–10 action potentials and an approximately twofold higher SNR, but these values are around tenfold lower than those for GCaMP6s (Supplementary Fig. 9a–d). The near-linear stimulus response over the range of approximately 2–40 stimuli is consistent with the near-unity Hill coefficient[11]. In cells, the rise and decay times of NIR-GECO1 appeared substantially slower than those of GCaMP6s. This observation is inconsistent with the fast Ca^{2+}-dissociation kinetics measured in vitro (Ca^{2+}-dissociation kinetic constant $k_{off}=1.93\ s^{-1}$ for NIR-GECO1 versus 1.08 s^{-1} for GCaMP6s; Supplementary Fig. 6b). With no targeting sequence attached, NIR-GECO1 distributes throughout the cytoplasm and nucleus. Measuring from the cell body, we found that nuclear-excluded NIR-GECO1 (NES-NIR-GECO1) exhibited similar kinetics as NIR-GECO1, ruling out slow Ca^{2+} diffusion in and out of the nucleus as an explanation for slower response kinetics (Supplementary Fig. 9c,d). When coexpressed in cultured neurons, NIR-GECO1 and GCaMP6s both reported spontaneous oscillations in Ca^{2+} concentration with opposite fluorescence changes (Supplementary Fig. 9e,f).

To evaluate in vivo expression of NIR-GECO1, we induced expression of the gene in layer 2/3 (L2/3) of mouse motor cortex via in utero electroporation (IUE). Imaging of brain slices revealed fluorescence through neuronal cell bodies and processes (Fig. 2a and Supplementary Fig. 8b) and no punctate structures. Stimulation of action potentials with whole-cell patch-clamp electrophysiology gave $-\Delta F/F_0$ of 7.2 ± 2.8%, 13.4 ± 3.8% and 27.6 ± 2.8% for 5, 10 and 20 action potentials, respectively (Fig. 2b, Supplementary Fig. 8c). Stimulation of neuronal activity with 4-aminopyridine resulted in mean maximal $-\Delta F/F_0$ of ~20% and mean averaged $-\Delta F/F_0$ of ~10% (Fig. 2c,d). To determine whether NIR-GECO1 could be used for one-photon in vivo imaging, we injected adeno-associated virus (AAV) carrying the NIR-GECO1 gene (AAV2/9-hSyn1-NIR-GECO1) in the sensorimotor cortex of mice. Mesoscale fluorescence imaging through the intact skin (hair removed) and skull of anesthetized mice during two paradigms of paw stimuli revealed transient stimuli- and NIR-GECO1-dependent fluorescence changes (decreases) of approximately 0.3% (Fig. 2e–g, Supplementary Figs. 10 and 11 and Supplementary Videos 1 and 2). Under similar conditions, GCaMP6s exhibited approximately tenfold greater fluorescence changes (increases). We attribute the better performance of GCaMP6s to its inherently larger Ca^{2+}-dependent fluorescence response (×30 versus ×8 under identical conditions; Supplementary Table 1), its higher Hill coefficient (2.4 versus 1.0) and lower K_d (144 versus 215 nm) that has been empirically optimized for neuronal activity imaging.

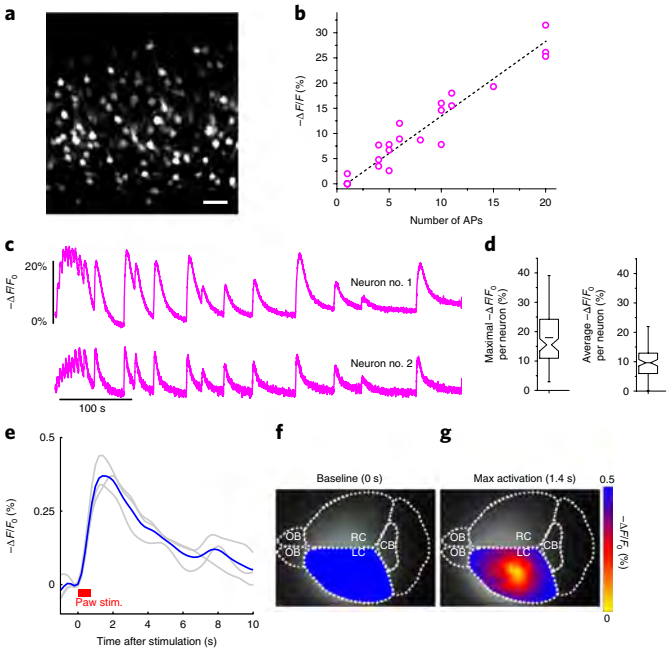

Fig. 2 | Imaging of in vivo expressed NIR-GECO1. a, Representative confocal image of live brain slice expressing NIR-GECO1 (641 nm Ex; 664LP Em; $n = 4$ slices from two mice at P11–22). Scale bar, 50 µm. **b**, NIR-GECO1 fluorescence responses to action potential (AP) trains evoked by current injections ($n = 6$ neurons from four mice at P11–22; dashed line indicates linear regression). **c**, Single-trial wide-field imaging of 4-aminopyridine (1 mM final concentration) evoked neuronal activity from the cell bodies of two representative neurons (631/28 nm Ex and 664LP Em; acquisition rate 20 Hz; $n = 129$ neurons from two slices from one mouse). **d**, Maximal (left) and average (right) $-\Delta F/F_0$ for the experiment of **c**. Box plots are used as described in Fig. 1g. For experiments in **a–d**, NIR-GECO1 was expressed in vivo by IUE at E15.5. **e–g**, In vivo mesoscale imaging of foot-shock responses in mouse sensorimotor cortex. Three mice (4 weeks old) were injected with AVV2/9-hSyn1-NIR-GECO1 in either the right or the left side of the brain and imaged (671 nm Ex; 721/42 nm Em) 10–21 d later. **e**, Response to a paw stimulation paradigm of ten pulses in 700 ms (0.5 mA, 20 ms on and 50 ms off). Each gray line represents the averaged response of a mouse across 19 cycles, and the blue line represents the mean response from all three mice ($n = 3$; that is, 57 cycles). **f**, Activation map of mouse brain, injected in left cortex, before stimulation. Diffuse fluorescence in the right cortex is attributed to diffusion of viral particles and light scattering. **g**, Activation map of mouse brain at max activation 1.4 s after stimulation. Scale bar, 2 mm. OB, olfactory bulb; CB, cerebellum; L/RC, left or right cortex.

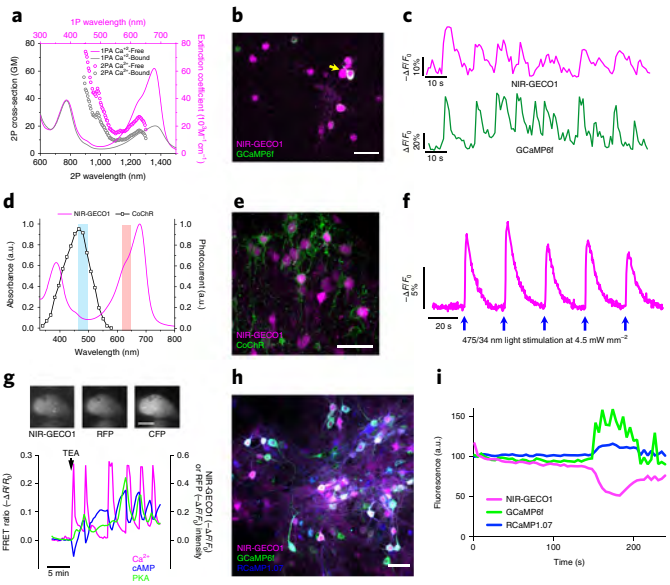

Fig. 3 | Spectral multiplexing of NIR-GECO1 with optogenetic indicators and actuators. a, One-photon (solid line; identical to Fig. 1c) and two-photon (open circles) absorption spectra of NIR-GECO1 in the presence and absence of Ca^{2+}. Two-photon absorption spectra are presented versus laser wavelength used for excitation. GM, Goeppert–Mayer units. **b**, Representative fluorescence image of cultured neurons expressing NIR-GECO1 (magenta) and GCaMP6f (green) acquired under two-photon excitation (imaging condition: NIR-GECO1 1,250 nm Ex, 705/90 nm Em; GCaMP6f 920 nm Ex, 518/45 nm Em; $n = 2$ cultures). Scale bar, 50 µm. **c**, Representative single-trial fluorescence recording of 4-aminopyridine (1 mM final concentration) evoked neuronal activity using NIR-GECO1 and GCaMP6f under imaging conditions as in **b** ($n = 32$ neurons from two cultures; yellow arrow indicates the neuron the fluorescence traces were obtained from; image acquisition rate, 1 Hz). **d**, Action spectrum of channelrhodopsin from *Chloromonas oogama* (CoChR) (black line; adapted with permission from ref. [12]) and NIR-GECO1 absorbance spectrum (magenta line; identical to Fig. 1c with no free Ca^{2+}) with wavelengths used for CoChR activation (475/34 nm; cyan bar) and NIR-GECO1 excitation (638/14 nm; orange bar). **e**, Representative confocal images of neurons in L2/3 of motor cortex coexpressing NIR-GECO1 (magenta) and CoChR-mTagBFP2-Kv2.2$_{motif}$ (green) targeted by IUE at E15.5 (imaging conditions: NIR-GECO1 641 nm Ex, 664LP Em; CoChR-mTagBFP2-Kv2.2$_{motif}$ 405 nm Ex and 452/45 nm Em). Scale bar, 50 µm. **f**, Single-trial wide-field imaging of NIR-GECO1 responses to CoChR activation (fluorescence excitation and activation as in **d**; 664LP Em; blue arrows, CoChR stimulation with 200 ms light pulses; image acquisition rate 5 Hz). Similar results were obtained with CheRiff[20] (Supplementary Fig. 13d,e). **g**, Top, representative fluorescence images of MIN6 β-cell coexpressing AKAR4 (left, 420/20 nm Ex and 475/40 nm Em for CFP and 535/25 nm Em for YFP), *NIR-GECO1* (middle, 640/30 nm Ex and 700/75 nm Em) and Pink Flamindo[16] (right, 555/25 nm Ex and 605/52 nm Em). Scale bar, 10 µM. Bottom, simultaneous visualization of Ca^{2+} (*NIR-GECO1*; $-\Delta F/F_0$, magenta line), cyclic AMP (Pink Flamindo; $\Delta F/F_0$, blue line), and PKA (AKAR4; FRET emission ratio $\Delta R/R_0$, green line) in a MIN6 cell treated with 20 mM tetraethylammonium chloride (TEA) at $t = 0$ (arrow). Traces for four additional representative cells are provided in Supplementary Fig. 14. **h**, Representative overlaid fluorescence image of dissociated neurons coexpressing NIR-GECO1, GCaMP6f and RCaMP1.07. **i**, Simultaneous detection of spontaneous neuronal activity reported by GCaMP6f, RCaMP1.07 and NIR-GECO1, in a single cell as in **h**. The percentage of responding cells (during a 3-min imaging session) was 92% for GCaMP6f ($n = 271$ neurons), 79% for RCaMP1.07 ($n = 178$ neurons) and 59% for NIR-GECO1 ($n = 331$ neurons).

Owing to its spectrally distinct fluorescence, NIR-GECO1 should be particularly useful for in vitro imaging in combination with optogenetic actuators and fluorescent-protein-based indicators. To explore such applications, we attempted two-photon imaging of NIR-GECO1 and GCaMP6f. NIR-GECO1 two-photon brightness at both 1,250 nm and 880 nm excitation is sufficient to image neurons in culture and in mouse brain tissue ex vivo and in vivo (Fig. 3a,b and Supplementary Fig. 12). With 1,250-nm excitation we observed neuronal-activity-dependent changes in NIR-GECO1 fluorescence in cultured neurons, as confirmed by coexpression of GCaMP6f, with average $-\Delta F/F_0$ of 48 ± 28% ($n = 37$ neurons from one culture; Fig. 3c). With two-photon excitation at 880 nm (11.4 mW of total light power), both the intracellular brightness and the photostability of NIR-GECO1 ($t_{1/2} = 20$ s) were slightly higher than those of miRFP, but lower than those of iRFP682 (Supplementary

Fig. 12a,b). However, when we used 880-nm excitation, we did not observe characteristic fluorescence changes of NIR-GECO1 associated with neuronal Ca^{2+} dynamics in neurons either in culture or in live brain slices (Supplementary Fig. 12c). We have not succeeded in demonstrating in vivo imaging of neuronal activity using NIR-GECO1 with either 880-nm or 1,250-nm two-photon excitation.

To explore the combined use of NIR-GECO1 and an optogenetic actuator, we prepared live brain slices expressing NIR-GECO1 and the high-photocurrent channelrhodopsin CoChR[12,13] (Fig. 3d). Activation of CoChR with cyan-colored light produced Ca^{2+} transients that were reliably reported by NIR-GECO1 (Fig. 3e,f), and there was no evidence of photophysical artifacts attributable to the illumination conditions (Supplementary Fig. 13a–c)[14].

To demonstrate NIR-GECO1's utility for use with fluorescent-protein-based indicators, we performed three-indicator (four-color) imaging using NIR-GECO1, the cyan- and yellow-fluorescent-protein-based protein kinase A indicator AKAR4[15] and the red-fluorescent-protein-based cAMP indicator Pink Flamindo[16]. Pharmacological stimulation of Ca^{2+} oscillations in MIN6 β-cells in vitro led to rapid and synchronous oscillations in Ca^{2+}, cAMP and PKA activity (Fig. 3g, Supplementary Fig. 14 and Supplementary Video 3). Coexpression of NIR-GECO1 with GCaMP6f[17] and RCaMP1.07[18] enabled three-color in vitro imaging of spontaneous neuronal activity (Fig. 3h,i and Supplementary Video 4).

We have demonstrated that NIR-GECO1 is a useful new addition to the GECI palette. As a first-generation indicator, NIR-GECO1 falls short of the most extensively optimized fluorescent-protein-based GECIs in several critical performance parameters. Accordingly, NIR-GECO1 is not generally useful for in vivo imaging of neuronal activity. However, NIR-GECO1 does provide a robust inverse response to Ca^{2+} concentration changes in cultured cells, primary neurons and acute slices roughly on par with GCaMP3. In addition, because of its highly red-shifted excitation maximum, it is the preferred Ca^{2+} indicator for pairing with blue-light-activated optogenetic actuators, to minimize actuator activation during imaging[19]. Finally, it creates a multitude of new opportunities for multiparameter imaging in conjunction with multiple fluorescent-protein-based intensiometric or ratiometric FRET-based indicators.

As with many BV-FPs, NIR-GECO1 is substantially dimmer than state-of-the-art fluorescent-protein-derived GECIs such as GCaMP6s (10.7 times brighter)[17] and jRGECO1a (three times brighter)[19]. To enable general utility for in vivo imaging, future iterations of NIR-GECO1 should be optimized for brighter fluorescence (for example, improved biliverdin-binding efficiency could provide up to an approximately fivefold increase), increased affinity for Ca^{2+}, increased photostability and faster kinetics. We expect NIR-GECO1 to be just as amenable to further improvements as the GCaMP series, and for these advancements to be soon realized through protein-engineering efforts.

Online content

Any methods, additional references, Nature Research reporting summaries, source data, statements of data availability and associated accession codes are available at https://doi.org/10.1038/s41592-018-0294-6.

Received: 10 May 2018; Accepted: 4 December 2018;
Published online: 21 January 2019

References

1. Tsien, R. Y. *Annu. Rev. Biochem.* **67**, 509–544 (1998).
2. Shu, X. et al. *Science* **324**, 804–807 (2009).
3. Rodriguez, E. A. et al. *Nat. Methods* **13**, 763–769 (2016).
4. Piatkevich, K. D. et al. *Biophys. J.* **113**, 2299–2309 (2017).
5. Shcherbakova, D. M., Stepanenko, O. V., Turoverov, K. K. & Verkhusha, V. V. *Trends Biotechnol.* **36**, 1230–1243 (2018).
6. Yu, D. et al. *Nat. Methods* **12**, 763–765 (2015).
7. Wagner, J. R., Zhang, J., Brunzelle, J. S., Vierstra, R. D. & Forest, K. T. *J. Biol. Chem.* **282**, 12298–12309 (2007).
8. Tian, L. et al. *Nat. Methods* **6**, 875–881 (2009).
9. Shcherbakova, D. M. & Verkhusha, V. V. *Nat. Methods* **10**, 751–754 (2013).
10. Piatkevich, K. D. et al. *Nat. Chem. Biol.* **14**, 352–360 (2018).
11. Inoue, M. et al. *Nat. Methods* **12**, 64–70 (2015).
12. Shemesh, O. A. et al. *Nat. Neurosci.* **20**, 1796–1806 (2017).
13. Klapoetke, N. C. et al. *Nat. Methods* **11**, 338–346 (2014).
14. Wu, J. et al. *ACS Chem. Neurosci.* **4**, 963–972 (2013).
15. Depry, C., Allen, M. D. & Zhang, J. *Mol. Biosyst.* **7**, 52–58 (2011).
16. Harada, K. et al. *Sci. Rep.* **7**, 7351 (2017).
17. Chen, T.-W. W. et al. *Nature* **499**, 295–300 (2013).
18. Ohkura, M., Sasaki, T., Kobayashi, C., Ikegaya, Y. & Nakai, J. *PLoS ONE* **7**, e39933 (2012).
19. Dana, H. et al. *eLife* **5**, e12727 (2016).
20. Hochbaum, D. R. et al. *Nat. Methods* **11**, 825–833 (2014).

Acknowledgements

The authors thank the University of Alberta Molecular Biology Services Unit; Y. Li, H. Zhou and A. Aggarwal, for technical support; A. Holt for providing access to the stopped-flow spectrophotometer; and M. Vanni, T. Murphy, A. Nimmerjahn and S. Chen for preliminary AAV testing. We thank M.-E. Paquet at the University of Laval Molecular Tools Platform and the Janelia Research Campus (JRC) Virus core for AAV production, We thank V. Rancic and the JRC Histology group for preparing cultured neurons. We thank D. Park and H.J. Suk for help with characterization of NIR-GECO1 in brain-slice and two-photon imaging. We thank M. Reiss for assistance with the mouse handling, X.L. Deán-Ben for help with the in vivo mesoscale data analysis, M. Davidson and X. Shu for the mIFP gene, and E. Rodriguez for the smURFP gene. Work in R.E.C.'s lab was supported by grants from NSERC (RGPIN 288338-2010), CIHR (MOP 123514 and FS 154310), Brain Canada and NIH (UO1 NS090565). D.R. acknowledges support from the European Research Council (ERC-2015-CoG-682379). The work of D.R. and S.S was also supported by the NIH (R21-EY026382 and UF1-NS107680). Work in J.Z.'s lab was supported by NIH (R01-DK073368 and R35-CA197622). E.S.B. was supported by J. Doerr, the HHMI-Simons Faculty Scholars Program, the Open Philanthropy Project, Human Frontier Science Program (RGP0015/2016), US Army Research Laboratory and the US Army Research Office (W911NF1510548), US-Israel Binational Science Foundation (2014509) and NIH (2R01-DA029639 and 1R01-GM104948).

Author contributions

Y.Q. developed NIR-GECO1 and performed in vitro characterization. Y.Q., K.D.P., A.S.A. and M.H.M. performed characterization in hippocampal neurons. K.D.P. and M.H.M. characterized NIR-GECO1 in intact brain slices. B.M.L. and S.G. performed in vivo mesoscale imaging. S.M. performed live-cell imaging in MIN6 β-cells. R.S.M. and M.D. measured two-photon spectra. W.Z. built the pcDuEx2 vector. Y.C. and J.W. worked on development of the smURFP-based GECI. M.D., T.E.H., J.Z., E.R.S., S.S., D.R., E.S.B. and R.E.C. supervised research. All authors were involved in data analysis. Y.Q., K.D.P. and R.E.C. wrote the manuscript.

Competing interests

The University of Alberta has non-exclusively licensed NIR-GECO1 to LumiSTAR Biotechnology.

Additional information

Supplementary information is available for this paper at https://doi.org/10.1038/s41592-018-0294-6.

Reprints and permissions information is available at www.nature.com/reprints.

Correspondence and requests for materials should be addressed to R.E.C.

Publisher's note: Springer Nature remains neutral with regard to jurisdictional claims in published maps and institutional affiliations.

Methods

General methods and materials. Synthetic DNA oligonucleotides were purchased from Integrated DNA Technologies. Q5 high-fid lity DNA polymerase (New England Biolabs) was used for routine PCR amplifi ations, and Taq DNA polymerase (New England Biolabs) was used for error-prone PCR. The QuikChange mutagenesis kit (Agilent Technologies) was used for site-directed mutagenesis. Restriction endonucleases, rapid DNA ligation kits and GeneJET miniprep kits were from Thermo Fisher Scientific. PCR roducts and products of restriction digests were purifi d using agarose gel electrophoresis and the GeneJET gel extraction kit (Thermo Fisher Scientific). ll DNA sequences were confi med using the BigDye Terminator v.3.1 cycle sequencing kit (Applied Biosystems). Reactions were analyzed at the University of Alberta Molecular Biology Service Unit. Absorbance measurements were made with a DU-800 UV-visible spectrophotometer (Beckman), and fluorescence spectra were recorded on a Safi e2 platereader (Tecan).

Engineering of NIR-GECO1. The gene encoding mIFP (a gift from Michael Davidson and Xiaokun Shu; Addgene plasmid no. 54,620)[6] was inserted between BamH1 and EcoR1 of a pBAD vector (Life Technologies) that expressed cyanobacteria *Synechocystis* HO-1 to convert an endogenous heme in bacteria into biliverdin, as previously described[3,21].

The DNA sequence encoding CaM and RS20 (a peptide that corresponds to the CaM-binding peptide of smooth muscle myosin light chain kinase; VDSSRRKWNKAGHAVRAIGRLSS) portions of REX-GECO1 (ref. [22]), with mutations Q306D and M339F borrowed from jRGECO1a[19], were genetically fused by overlap extension PCR using a DNA sequence that encodes for the flexible peptide linker GGGGS[23].

For each site (X) of mIFP targeted for CaM-RS20 insertion, the full-length gene (encoding $mIFP_{1\ to\ X}$-CaM-RS20-$mIFP_{X+1\ to\ 320}$) was assembled by overlap extension PCR and then inserted into the pBAD vector. Variants were expressed in *E. coli* strain DH10B (Thermo Fisher Scientific) in LB media supplemented with 100 μg ml^{-1} ampicillin and 0.0016% L-arabinose. Proteins were extracted using B-PER bacterial protein extraction reagent (Thermo Fisher Scientific) and tested for fluorescence brightness and Ca^{2+}-dependent response.

The most promising variant was subjected to an iterative process of library generation and screening in *E. coli*. The pBAD vector was used in the first three rounds. From the fourth round, pcDuEx2 was used to enable expression in both *E. coli* and mammalian cells. Libraries were generated by error-prone PCR of the whole gene[24] or site-directed mutagenesis using Quikchange (Agilent Technologies) and degenerate codons at the targeted positions.

For libraries generated by random mutagenesis, approximately 10,000 colonies were screened in a given round. For libraries generated by randomization of one or more codons, a number of colonies that was approximately threefold the theoretical number of gene variants were screened. For each round, the top 2% of colonies with high fluorescence intensity were picked, cultured and tested on 396-well plates. Approximately 25% of those picked variants were further screened in HeLa cells on the basis of fluorescence. In a given round, screening was stopped when a substantially improved variant was identified. There were 12 rounds of screening before NIR-GECO1 was identified.

NIR-GECO1 expression vectors. pcDuEx2 was constructed based on the pcDNA3.1 backbone. The Tac promoter and a gene sequence containing Kpn2I and XbaI sites was inserted immediately after the CMV promoter by overlap extension PCR. A DNA fragment containing the T7 promoter, the gene encoding NIR-GECO1 and the gene encoding HO-1 was amplified from the pBAD vector and inserted into the Kpn2I and XbaI sites.

For HeLa cell expression, the pcDuEx2 vector was used. For expression in dissociated neurons, either an AAV2 vector or a lentivirus containing NIR-GECO1 was used. For AAV2 vector preparation, NIR-GECO1 was cloned from pcDuEx2 into BamHI and HindIII sites of an AAV2 vector (a gift from Roger Tsien; Addgene plasmid no. 50970)[25]. To create lentivirus expressing NIR-GECO1, the gene for NIR-GECO1 or NIR-GECO1-T2A-HO1 was cloned into the BamHI and EcoRI sites of FCK lentivirus vector (Addgene plasmid no. 22217). HEK293FT cells at 80% confluency in 35-mm cell-culture dishes (Corning) were transfected with 1.5 μg of FCK-CMV-NIR-GECO1 or FCK-CMV-NIR-GECO1-T2A-HO1, 1.0 μg of psPAX2 (a gift from D. Trono; Addgene plasmid no. 12,260), 0.5 μg of pMD2.G (a gift from D. Trono; Addgene plasmid no. 12,259) and 0.2 μg of pAdvantage (Promega), with 9 μl of Turbofect transfection reagent in 2 ml of Opti-MEM medium (Thermo Fisher Scientific). Opti-MEM medium containing Turbofect and DNA mix were replaced with 2 ml of complete cell-culture medium containing 110 mg ml^{-1} sodium pyruvate at 24 h post-transfection. At 48 h post-transfection, the virus-containing supernatant was collected, spun at 400*g* (relative centrifugal force) for 5 min and filtered through a 0.45-μm PVDF syringe filter unit (EMD Millipore) to get rid of pellet cellular debris. Dissociated neurons in 24-well plates were transduced with 2 ml of virus-containing supernatant.

Protein purification and in vitro characterization. The gene encoding NIR-GECO1, with a poly-histidine tag on the C terminus, was expressed from the pBAD vector. Bacteria were lysed with a cell disruptor (Constant Systems Ltd) and then centrifuged at 15,000*g* for 30 min, and proteins were purified by Ni-NTA affinity chromatography (Agarose Bead Technologies). The buffer was typically exchanged to 10 mM MOPS, 100 mM KCl (pH 7.2) with centrifugal concentrators (GE Healthcare Life Sciences). We determined extinction coefficients by comparing the absorbance value at 678 nm to the absorbance value at the 391 nm and assuming an extinction coefficient of 39,900 $M^{-1}cm^{-1}$ at 391 nm[2,6]. For determination of quantum yields (Φ), purified mIFP (Φ = 0.08) was used as a standard. The concentration of NIR-GECO1 (Ca^{2+}-free), NIR-GECO1 (Ca^{2+}-saturated) and mIFP was adjusted to have absorbance of 0.2–0.6 at 650 nm. A series of dilutions, with absorbance ranging from 0.01 to 0.05, were prepared, and integrated emission intensity versus absorbance was plotted. Quantum yields were determined from the slopes (*S*) of each line using the equation $\Phi_{protein} = \Phi_{standard} \times (S_{protein}/S_{standard})$. We carried out pH titrations by diluting protein into buffers (pH from 2 to 11) containing 30 mM trisodium citrate, 30 mM sodium borate and either 10 mM $CaCl_2$ or 10 mM EGTA. Fluorescence intensities as a function of pH were then fitted by a sigmoidal binding function to determine the apparent pK_a. Ca^{2+} titrations were carried out using EGTA-buffered Ca^{2+} solutions (Calcium Calibration Buffer Kit no. 1, Life Technologies). We prepared buffers by mixing a CaEGTA buffer (30 mM MOPS, 100 mM KCl, 10 mM EGTA, 10 mM $CaCl_2$) and an EGTA buffer (30 mM MOPS, 100 mM KCl, 10 mM EGTA) to give free Ca^{2+} concentrations ranging from 0 nm to 39 μM at 25 °C. Fluorescence intensities were plotted against Ca^{2+} concentrations and fitted by a sigmoidal binding function to determine the Hill coefficient and K_d. To determine k_{off}, we used an SX20 stopped-flow spectrometer (Applied Photophysics). Briefly, protein samples with 10 μM $CaCl_2$ (30 mM MOPS, 100 mM KCl, pH 7.2) were rapidly mixed with 10 mM EGTA (30 mM MOPS, 100 mM KCl, pH 7.2) at room temperature, and an absorption growth curve was measured and fitted by a single exponential equation.

Two-photon spectra and cross-sections were measured using femtosecond excitation as described in Supplementary Note 2.

Animal care. For experiments performed at Massachusetts Institute of Technology (MIT), all methods for animal care and use were approved by the MIT Committee on Animal Care and were in accordance with the National Institutes of Health Guide for the Care and Use of Laboratory Animals. Four time pregnant Swiss Webster mice (Taconic) were used for this study, as were five C57BL/6 mice (Taconic), ages 4–12 weeks. Mice were used without regard to gender.

For experiments performed at Technical University of Munich, all animal in vivo experimentation was done in full compliance with the institutional guidelines of the Institute for Biological and Medical Imaging and with approval from the Government District of Upper Bavaria. A total of 12 mice were used for these experiments: 3 female FOXN1 nude mice that were injected with the NIR-GECO1 virus, 3 female FOXN1 nude mice that were injected with the miRFP virus, 3 female Black6 (C57BL/6J) transgenic mice expressing GCaMP6s, and 3 mice (2 female FOXN1 and 1 female Black6) that were injected with PBS as negative controls.

All experiments at University of Alberta for obtaining the cortical neurons were approved by the University of Alberta Animal Care and Use Committee and carried out in compliance with guidelines of the Canadian Council for Animal Care and the Society for Neuroscience's Policies on the Use of Animals and Humans in Neuroscience Research.

For experiments at HHMI Janelia Research Campus, all surgical and experimental procedures were in accordance with protocols approved by the HHMI Janelia Research Campus Institutional Animal Care and Use Committee and Institutional Biosafety Committee.

Imaging of NIR-GECO1 in HeLa cells and dissociated neuron cultures. HeLa cells (40–60% confluent) in 24-well glass-bottom plates (Cellvis) were transfected with 0.5 μg of the NIR-GECO1-pcDuEx2 plasmid and 2 μl of TurboFect (Thermo Fisher Scientific) in Dulbecco's modified Eagle's medium (DMEM; Gibco Fisher Scientific). Following 2 h of incubation, the media was changed to DMEM supplemented with 10% fetal bovine serum (FBS; Sigma-Aldrich), 2 mM GlutaMax (Thermo Fisher Scientific) and 1% penicillin–streptomycin (Gibco). The cells were then incubated for 48 h at 37 °C in a CO_2 incubator. Before imaging, culture medium was changed to Hanks' Balanced Salt Solution (HBSS).

For dissociated hippocampal mouse neuron culture preparation, postnatal day 0 or 1 Swiss Webster mice (Taconic Biosciences) were used as previously described[10]. Briefly, dissected hippocampal tissue was digested with 50 units of papain (Worthington Biochem) for 6–8 min at 37 °C, and the digestion was stopped by incubation with ovomucoid trypsin inhibitor (Worthington Biochem) for 4 min at 37 °C. Tissue was gently dissociated with Pasteur pipettes, and dissociated neurons were plated at a density of 20,000–30,000 per glass coverslip coated with Matrigel (BD Biosciences). Neurons were seeded in 100 μl of plating medium containing MEM (Life Technologies), glucose (33 mM; Sigma), transferrin (0.01%; Sigma), HEPES (10 mM; Sigma), Glutagro (2 mM; Corning), insulin (0.13%; Millipore), B27 supplement (2%; Gibco) and heat-inactivated FBS (7.5%; Corning). After cell adhesion, additional plating medium was added. AraC (0.002 mM; Sigma) was added when glia density was 50–70% of confluence. Neurons were grown at 37 °C and 5% CO_2 in a humidified atmosphere. We

transduced cultured neurons at 4–5 days in vitro (DIV) by administering ~10^{10} viral particles of rAAV8-hSyn-iRFP682, rAAV8-hSyn-miRFP (both from Vector Core, University of North Carolina) or rAAV9-hSyn-NIR-GECO1 (Department of Biochemistry and Microbiology, University of Laval) per well (the rAAV genome titer was determined by dot blot). For coexpression of the GECIs, the rAAV8-hSyn-GCaMP6f, rAAV8-hSyn-RCaMP1.07 (both from Vector Core, University of North Carolina) and rAAV9-hSyn-NIR-GECO1 viral particles were added in a 1/1/3 ratio, respectively. A biliverdin hydrochloride (Sigma-Aldrich) solution in dimethylsulfoxide (25 mM) was used as a 1,000× stock (25 µM final concentration) for the experiments shown in Fig. 1g and Supplementary Fig. 7a,b. All measurements on neurons were taken after DIV 16.

For dissociated rat cortical neuron culture preparation, postnatal day 0 or 1 Sprague Dawley rats were used. Dissected cortices were digested in Papain solution (50 units; Sigma) for 10 min at 37 °C and then incubated with DNase (0.15 mg ml^{-1}; Sigma) for 5 min at 37 °C. After washing the tissue with FBS (Sigma) and removing supernatant, we added neurobasal B27 (Thermo Fisher Scientific) to tissue. Tissue was then gently dissociated with Pasteur pipettes, and dissociated neurons were plated at a density of ~1.5×10^5 on collagen-coated 24-well glass-bottom dishes containing NbActiv4 culture medium (BrainBits LLC) supplemented with 2% FBS, penicillin-G potassium salt (50 units per ml), and streptomycin sulfate (50 mg ml^{-1}). Half of the culture media was replaced every 4–5 d. Neuronal cells were infected using the NIR-GECO1 lentivirus on day 8. Before imaging, the culture medium was changed to HBSS.

Wide-field fluorescence imaging of cultured neurons was performed using an epifluorescence inverted microscope (Eclipse Ti-E, Nikon) equipped with a Photometrics QuantEM 512SC camera and a 75-W Nikon xenon lamp or a Zyla5.5 sCMOS (scientific complementary metal-oxide semiconductor) camera (Andor) and a SPECTRA X light engine (Lumencor). NIS-Elements Advanced Research (Nikon) was used for automated microscope and camera control. Cells were imaged with 60×/1.49-NA (numerical aperture) oil or 20×/0.75-NA air objective lenses (Nikon) at room temperature. For dual-color imaging with GCaMP6s, NIR (650/60 nm Ex and 720/50 nm Em) and green (490/15 nm Ex and 525/50 nm Em) filter sets were rotated into the emission light path. Three-color Ca imaging with GCaMP6f and RCaMP1.07 was performed using an inverted Nikon Eclipse Ti microscope equipped with a spinning disk sCSUW1 confocal scanner unit (Yokogawa), 488-, 561- and 642-nm solid state lasers, 525/25-nm, 579/34-nm and 664LP emission filters, a 20×/0.75-NA air objective lens (Nikon) and a 4.2 PLUS Zyla camera (Andor), controlled by NIS-Elements AR software. One cautionary note for confocal imaging is that gallium-arsenide-phosphide photomultiplier tube detectors have poor sensitivity at wavelengths greater than 700 nm.

Two-photon imaging (as shown in Fig. 3b,c and Supplementary Fig. 12c) was performed using an Olympus FVMPE-RS equipped with two lasers for fluorescence excitation. An InSight X3 laser (Spectra-Physics) tuned to 1,250 nm at 8.0% transmissivity was used to excite NIR-GECO1, and a Mai-Tai HP Ti:Sapphire laser (Spectra-Physics) tuned to 920 nm at 17.4% transmissivity was used to excite GCaMP6f. The laser beams were focused by a 25×/1.05-NA water-immersion objective lens (Olympus). NIR-GECO1 emission was separated using a 660–750-nm filter, GCaMP6f emission was separated using a 495–540-nm filter, and signals were collected onto separate photomultiplier tubes. Imaging was performed at a sampling speed of 2.0 µs per pixel with one-way galvano scanning. Raw scanner data were converted to an image z-stack using ImageJ (NIH).

Two-photon imaging for Supplementary Fig. 12a,b,d–f was performed using a two-photon laser scanning microscope (Ultima IV, Prairie Technologies) with a mode-locked Ti-Sapphire laser (Mai-Tai, Spectra-Physics) and a 16×/0.8-NA water-immersion objective (CFI75 LWD 16; Nikon). For image acquisition, the laser was set to emit 880 nm at a total light power of 11.4 mW, and 535/50-nm and 731/137-nm emission filters (Semrock) were used. The microscope was operated using the ScanImage 3.8 software package[26].

Electrophysiology and Ca^{2+} imaging in dissociated hippocampal neurons. The genes encoding NIR-GECO1 and GCaMP6s were expressed under the control of a synapsin promoter in cultured rat hippocampal neurons. Neurons were stimulated using a custom-built field stimulator using a stimulus isolator (A385, World Precision Instruments) with platinum wires. Field stimuli (50 V, 83 Hz, 1 ms) were delivered in trains of 1, 2, 3, 5, 10, 20, 40, 80, 120 and 160 to the cultured neurons. Neurons were imaged using a Nikon Eclipse Ti2 inverted microscope equipped with a 40×/1.4-NA objective (Nikon). A quad bandpass filter (set number, 89,000; Chroma) was used along with a 480-nm light-emmitting diode (LED) (Spectra X light engine, Lumencor) or a 640-nm LED (Spectra X light engine, Lumencor) to image GCaMP6s or NIR-GECO1, respectively. Fluorescence was collected using an sCMOS camera (Orca-Flash4.0, Hamamatsu) at 34 Hz. For GCaMP6s, the response amplitude ($\Delta F/F_{min}$) was quantified as the change in fluorescence divided by baseline fluorescence over the 0.5-s period preceding the stimulus. For NIR-GECO1, the response amplitude was quantified as the change in fluorescence divided by peak fluorescence during the stimulus ($-\Delta F/F_{min}$). SNR was quantified as the peak change in fluorescence over the s.d. of the signal over the 0.5-s period preceding stimulation.

Multiplexed live-cell imaging with NIR-GECO1 in MIN6 β-cells. MIN6 pancreatic β-cells were cultured in DMEM containing 4.5 g l^{-1} glucose, supplemented with 10% (v/v) FBS, 1% (v/v) Pen-Strep and 50 µM β-mercaptoethanol, and maintained at 37 °C with a 5% CO_2 atmosphere. Cells were plated onto 35-mm glass-bottom dishes, grown to 40–60% confluence and then transfected with 0.5 µg each of plasmids encoding AKAR4[15], Pink Flamindo[16] and NIR-GECO1 using Lipofectamine 2000 (Invitrogen). After 48 h, cells were washed twice with HBSS (Gibco) and imaged in HBSS at 37 °C using a Zeiss AxioObserver Z1 inverted epifluorescence microscope (Carl Zeiss) equipped with a 40×/1.3-NA objective, a Lambda 10–2 filter-changer (Sutter Instruments) and a Photometrics Evolve 512 EMCCD (electron-multiplying charge-coupled device) (Photometrics) controlled by METAFLUOR v.7.7 software (Molecular Devices). Filters for cyan/yellow emission ratio were a 420DF20 excitation filter, a 450DRLP dichroic mirror and two emission filters (475DF40 for CFP and 535DF25 for YFP). Filters for RFP were a 555DF25 excitation filter, a ZT568RDC dichroic mirror and a 605DF52 emission filter. Filters for NIR-GECO1 were a 640DF30 excitation filter, a 700DF75 excitation filter and a T660LPXR dichroic mirror. Exposure times ranged between 50 and 500 ms, with EM gain set from 10–50, and images were acquired every 20 s. Fluorescence intensities were corrected by background subtraction. The emission ratio change ($R - R_0$) or fluorescence intensity change ($F - F_0$) was divided by the initial ratio or intensity to obtain $\Delta R/R_0$ or $\Delta F/F_0$, with time zero defined as the time point immediately preceding drug addition. Graphs were plotted using GraphPad Prism 7 (GraphPad Software).

In utero electroporation. Embryonic day (E) 15.5 timed-pregnant female Swiss Webster (Taconic) mice were deeply anesthetized with 2% isoflurane. Uterine horns were exposed and periodically rinsed with warm sterile PBS. A plasmid encoding NIR-GECO1 or a mixture of plasmids encoding NIR-GECO1 and CoChR (pCAG-NIR-GECO1-WPRE, pCAG-CoChR-mTagBFP2-Kv2.2motif-WPRE; at a total DNA concentration of ~1–2 µg µl^{-1}) diluted with PBS were injected into the lateral ventricle of one cerebral hemisphere of an embryo. Five voltage pulses (50 V, 50-ms duration, 1 Hz) were delivered using round plate electrodes (ECM 830 electroporator, Harvard Apparatus). Injected embryos were placed back into the dam, and allowed to mature to delivery. The P0 pups were screened for corresponding fluorescence and negative pups were excluded for further experiments. All experimental manipulations were performed in accordance with protocols approved by the Massachusetts Institute of Technology Committee on Animal Care, following guidelines described in the US National Institutes of Health Guide for the Care and Use of Laboratory Animals.

Acute brain slice preparation. Acute brain slices were obtained from Swiss Webster (Taconic) mice at P11 to P22, using standard techniques. Mice were used without regard for sex. No statistical methods were used to estimate sample size for animal studies throughout. No randomization or blinding were used for animal studies throughout. Mice were anaesthetized by isoflurane inhalation, decapitated and cerebral hemispheres were quickly removed and placed in cold choline-based cutting solution consisting of (in mM): 110 choline chloride, 25 $NaHCO_3$, 2.5 KCl, 7 $MgCl_2$, 0.5 $CaCl_2$, 1.25 NaH_2PO_4, 25 glucose, 11.6 ascorbic acid and 3.1 pyruvic acid (339–341 mOsm per kg; pH 7.75 adjusted with NaOH) for 2 min, blocked and transferred into a slicing chamber containing ice-cold choline-based cutting solution. Coronal slices (300 µm thick) were cut with a Compresstome VF-300 slicing machine, transferred to a holding chamber with artificial cerebrospinal fluid (ACSF) containing (in mM) 125 NaCl, 2.5 KCl, 25 $NaHCO_3$, 2 $CaCl_2$, 1 $MgCl_2$, 1.25 NaH_2PO_4 and 11 glucose (300–310 mOsm per kg; pH 7.35 adjusted with NaOH) and recovered for 10 min at 34 °C followed by another 30 min at room temperature. Slices were subsequently maintained at room temperature until use. Both cutting solution and ACSF were constantly bubbled with 95% O_2 and 5% CO_2.

Concurrent electrophysiology and Ca^{2+} imaging in acute brain slice. Slices were transferred to a recording chamber on an Olympus BX51WI upright microscope and superfused (2–3 ml min^{-1}) with ACSF at room temperature. Whole-cell patch-clamp recordings were acquired via an Axopatch 700B amplifier (Molecular Devices) and Digidata 1440 digitizer (Molecular Devices). For recordings, borosilicate glass pipettes (Warner Instruments) with an outer diameter of 1.2 mm and a wall thickness of 0.255 mm were pulled to a resistance of 3–5 MΩ with a P-97 Flaming/Brown micropipette puller (Sutter Instruments) and filled with a solution containing 155 mM K-gluconate, 8 mM NaCl, 0.1 mM $CaCl_2$, 0.6 mM $MgCl_2$, 10 mM HEPES, 4 mM Mg-ATP and 0.4 mM Na-GTP. The pipette solution pH was adjusted to 7.3 with KOH and the osmolarity was adjusted to 298 mOsm with sucrose. Cells were visualized through a 40×/0.8-NA water-immersion objective with epifluorescence. Whole-cell current-clamp recordings were obtained from NIR-GECO1-positive neurons in layer 2/3 of motor cortex. Fluorescence was excited by a SPECTRA X light engine (Lumencor) with 638/14-nm excitation filter (Semrock), fluorescence was collected through the same objective, passed through a 664 LP emission filter and imaged onto an Orca-Flash4.0 v.2 sCMOS camera (Hamamatsu) at 50-Hz acquisition frequency.

In vivo imaging of NIR-GECO1. Methods for in vivo two-photon imaging to acquire the image shown in Supplementary Fig. 12f are provided as Supplementary Note 3. Methods for in vivo mesoscale imaging to acquire data

and images shown in Fig. 2e–g and Supplementary Figs. 10 and 11 are provided as Supplementary Note 4.

Statistics and reproducibility. All data are expressed as mean ± s.d. or mean ± s.e.m., as specified in figure legends. Box plots with notches[27] are used for Figs. 1g and 2d and Supplementary Figs. 7b, 12a and 13c. In these plots, the narrow part of the notch is the median; the top and bottom of the notch denote the 95% confidence interval of the median; the horizontal line is the mean; the top and bottom horizontal lines are the 25th and 75th percentiles for the data; and the whiskers extend 1.5 times the interquartile range from the 25th and 75th percentiles. Sample sizes (n) are listed with each experiment. No samples were excluded from analysis and all experiments were reproducible. For experiments for which representative data are shown, the number of times each experiment was repeated independently with similar results is summarized in Supplementary Note 5. No randomization or blinding was used. All attempts at replication of the experiments were successful.

Reporting Summary. Further information on research design is available in the Nature Research Reporting Summary linked to this article.

Data availability

The NIR-GECO1 gene sequence is available through GenBank (submission no. MK134690). pDuEx2-NIR-GECO1 (plasmid no. 113,680) and pAAV-hSyn-NES-NIR-GECO1 (plasmid no. 113,683) are available via Addgene according to the terms of the Uniform Biological Material Transfer Agreement. Source data for Figs. 1–3 and Supplementary Figs. 5–14 are available online.

References

21. Gambetta, G. A. & Lagarias, J. C. *Proc. Natl Acad. Sci. USA* **98**, 10566–10571 (2001).
22. Wu, J. et al. *Nat. Commun.* **5**, 5262 (2014).
23. Heckman, K. L. & Pease, L. R. *Nat. Protoc.* **2**, 924–932 (2007).
24. Cirino, P. C., Mayer, K. M. & Umeno, D. in *Directed Evolution Library Creation: Methods and Protocols* (eds Arnold, F. H. & Georgiou, G.) 3–9 (Humana, Totowa, NJ, 2003).
25. Lin, J. Y. et al. *Neuron* **79**, 241–253 (2013).
26. Pologruto, T. A., Sabatini, B. L. & Svoboda, K. *Biomed. Eng. Online.* **2**, 13 (2003).
27. Krzywinski, M. & Altman, N. *Nat. Methods* **11**, 119–120 (2014).

nature research

Corresponding author(s): Robert E. Campbell

Double-blind peer review submissions: write DBPR and your manuscript number here instead of author names.

Reporting Summary

Nature Research wishes to improve the reproducibility of the work that we publish. This form provides structure for consistency and transparency in reporting. For further information on Nature Research policies, see Authors & Referees and the Editorial Policy Checklist.

Statistical parameters

When statistical analyses are reported, confirm that the following items are present in the relevant location (e.g. figure legend, table legend, main text, or Methods section).

n/a	Confirmed	
☐	☒	The exact sample size (*n*) for each experimental group/condition, given as a discrete number and unit of measurement
☐	☒	An indication of whether measurements were taken from distinct samples or whether the same sample was measured repeatedly
☒	☐	The statistical test(s) used AND whether they are one- or two-sided *Only common tests should be described solely by name; describe more complex techniques in the Methods section.*
☒	☐	A description of all covariates tested
☒	☐	A description of any assumptions or corrections, such as tests of normality and adjustment for multiple comparisons
☐	☒	A full description of the statistics including central tendency (e.g. means) or other basic estimates (e.g. regression coefficient) AND variation (e.g. standard deviation) or associated estimates of uncertainty (e.g. confidence intervals)
☒	☐	For null hypothesis testing, the test statistic (e.g. *F*, *t*, *r*) with confidence intervals, effect sizes, degrees of freedom and *P* value noted *Give P values as exact values whenever suitable.*
☒	☐	For Bayesian analysis, information on the choice of priors and Markov chain Monte Carlo settings
☒	☐	For hierarchical and complex designs, identification of the appropriate level for tests and full reporting of outcomes
☒	☐	Estimates of effect sizes (e.g. Cohen's *d*, Pearson's *r*), indicating how they were calculated
☐	☒	Clearly defined error bars *State explicitly what error bars represent (e.g. SD, SE, CI)*

Our web collection on statistics for biologists may be useful.

Software and code

Policy information about availability of computer code

Data collection	Molecular Devices MetaMorph and MetaFluor 7.7, NIS-Elements AR software, LabView, Andor Solis 4.21, OLYMPUS FLUOView 3000
Data analysis	Graphpad Prism 6.0 and 7.0, Origin9, Microsoft Excel, Clampfit 10.7, MatLab2017b, ImageJ, MetaFluor 7.7

For manuscripts utilizing custom algorithms or software that are central to the research but not yet described in published literature, software must be made available to editors/reviewers upon request. We strongly encourage code deposition in a community repository (e.g. GitHub). See the Nature Research guidelines for submitting code & software for further information.

Data

Policy information about availability of data

All manuscripts must include a data availability statement. This statement should provide the following information, where applicable:

- Accession codes, unique identifiers, or web links for publicly available datasets
- A list of figures that have associated raw data
- A description of any restrictions on data availability

One page 15 of the Supplementary Material we state: "Data Availability. Gene sequence data will be deposited in GenBank with accession codes that are TBD. Plasmids will be distributed via Addgene according to the terms of the Uniform Biological Material Transfer Agreement. Source data for Figs. 1-2, and Supplementary Figs. 5-7, 9, 11 will be included in the final version of the paper."

Field-specific reporting

Please select the best fit for your research. If you are not sure, read the appropriate sections before making your selection.

☒ Life sciences ☐ Behavioural & social sciences ☐ Ecological, evolutionary & environmental sciences

For a reference copy of the document with all sections, see nature.com/authors/policies/ReportingSummary-flat.pdf

Life sciences study design

All studies must disclose on these points even when the disclosure is negative.

Sample size	On page 9 of Supplementary Material we state: "No statistical methods were used to estimate sample size for animal studies throughout. " As noted Dell et al ILAR. J (2002) and recommended by the NIH, "In experiments based on the success or failure of a desired goal, the number of animals required is difficult to estimate..." As noted in the aforementioned paper, "The number of animals required is usually estimated by experience instead of by any formal statistical calculation, although the procedures will be terminated [when the goal is achieved]." On page 15 of the Supplementary Material we include the following statement: "Statistical analysis. All data are expressed as mean ± s.d or mean ± s.e.m, as specified in figure legends. Box plots with notches19 are used for Figs. 1g, 2d, and Supplementary Figs. 7b, 12a and 13c. In these plots, the narrow part of notch is the median; the top and bottom of the notch is the 95% confidence interval of the median; the horizontal line is the mean; the top and bottom horizontal lines are the 25% and 75% percentiles for the data; and the whiskers extend 1.5× the interquartile range from the 25th and 75th percentiles. Sample sizes (n) are listed with each experiment. No samples were excluded from analysis and all experiments were reproducible. No randomization or blinding was used "
Data exclusions	P31. The P0 pups were screened for corresponding fluorescence, negative pups were excluded for further experiments.
Replication	P33. All attempts at replication were successful.
Randomization	P33. No randomization or blinding was used
Blinding	P33. No randomization or blinding was used

Reporting for specific materials, systems and methods

Materials & experimental systems

n/a	Involved in the study
☒	☐ Unique biological materials
☒	☐ Antibodies
☐	☒ Eukaryotic cell lines
☒	☐ Palaeontology
☐	☒ Animals and other organisms
☒	☐ Human research participants

Methods

n/a	Involved in the study
☒	☐ ChIP-seq
☒	☐ Flow cytometry
☒	☐ MRI-based neuroimaging

Eukaryotic cell lines

Policy information about cell lines

Cell line source(s)	HeLa (ATCC), HEK293FT (Thermo Fisher Scientific), MIN6 (Miyazaki laboratory, Osaka University)
Authentication	Cell lines were not authenticated
Mycoplasma contamination	MIN6 cells were tested weekly for Mycoplasma using DNA staining. Other cell lines were not tested.
Commonly misidentified lines (See ICLAC register)	HEK293FT cells were used for production of lentivirus due to the following advantages: fast-growing, high transfection efficientcy and tolerance of high levels of proteins.

Animals and other organisms

Policy information about studies involving animals; ARRIVE guidelines recommended for reporting animal research

Laboratory animals	Pages 4 and 5 of Supplementary material. We state: "Animal care. For experiments performed at Massachusetts Institute of

Laboratory animals

Technology (MIT), all methods for animal care and use were approved by the MIT Committee on Animal Care and were in accordance with the National Institutes of Health Guide for the Care and Use of Laboratory Animals. Four time pregnant Swiss Webster mice (Taconic) were used for this study, as were five C57BL/6 mice (Taconic), ages 4–12 weeks. Mice were used without regard to gender.
For experiments performed at Technical University of Munich, all animal in vivo experimentation was done in full compliance with the institutional guidelines of the Institute for Biological and Medical Imaging and with approval from the Government District of Upper Bavaria. A total of twelve mice were used for these experiments: three female FOXN1 nude mice that were injected with the NIR-GECO1 virus; three female FOXN1 nude mice that were injected with the miRFP virus; three female Black6 (C57BL/6J) transgenic mice expressing GCaMP6s and three mice (two female FOXN1 and one female Black6) that were injected with PBS as negative controls.
All experiments at University of Alberta for obtaining the cortical neurons were approved by the University of Alberta Animal Care and Use Committee and carried out in compliance with guidelines of the Canadian Council for Animal Care and the Society for Neuroscience's Policies on the Use of Animals and Humans in Neuroscience Research.
For experiments at HHMI Janelia Research Campus, all surgical and experimental procedures were in accordance with protocols approved by the HHMI Janelia Research Campus Institutional Animal Care and Use Committee and Institutional Biosafety Committee."

Wild animals

The study did not involve wild animals.

Field-collected samples

The study did not involve sample collected from the field.

nature research

Corresponding author(s): Robert E. Campbell

Double-blind peer review submissions: write DBPR and your manuscript number here instead of author names.

☐ Initial submission ☒ Revised version ☐ Final submission

Editorial Policy Checklist

This form is used to ensure compliance with Nature Research editorial policies related to research ethics and reproducibility. For further information, please see our Authors & Referees site. All relevant questions on the form must be answered.

Competing interests

Policy information about competing interests

Competing interests declaration

In the interest of transparency and to help readers form their own judgements of potential bias, Nature Research journals require authors to declare any competing financial and/or non-financial interest in relation to the work described in the submitted manuscript.

☐ No, I declare that the authors have no competing financial or non-financial interests as defined by Nature Research.

☒ Yes, I declare that the authors have a competing interest as defined by Nature Research

The University of Alberta has non-exclusively licensed NIR-GECO1 to LumiSTAR Biotechnology.

Data availability

Policy information about availability of data

Data availability statement

All manuscripts must include a data availability statement. This statement should provide the following information, where applicable:

- Accession codes, unique identifiers, or web links for publicly available datasets
- A list of figures that have associated raw data
- A description of any restrictions on data availability

☒ A full data availability statement is included in the manuscript.

Mandated accession codes (where applicable)

Confirm that all relevant data are deposited into a public repository and that accession codes are provided.

☐ All relevant accession codes are provided ☒ Accession codes will be available before publication ☐ No data with mandated deposition

Data presentation

Image integrity

☒ Confirm that all images comply with our image integrity policy.

Unprocessed data must be provided upon request. Please double-check figure assembly to ensure that all panels are accurate (e.g. all labels are correct, no inadvertent duplications have occurred during preparation, etc.).

Data distribution

Present data in a format that shows data distribution (dot-plots or box-and-whisker plots).

Define all box-plot elements (e.g. center line, median; box limits, upper and lower quartiles; whiskers, 1.5x interquartile range; points, outliers).

If using bar graphs, overlay the corresponding dot plots.

☒ Confirm that all data presentation meets these requirements and that individual data points are shown.

Specific policy considerations

Some types of research require additional policy disclosures. Please indicate whether these apply to your study. If you are not certain, please read the appropriate section before selecting a response.

Does not apply	Involved in the study
☐	☒ Custom software or computer code
☒	☐ Macromolecular structural data
☐	☒ Research animals and/or animal-derived materials that require ethical approval
☒	☐ Human research participants
☒	☐ Clinical data

Code availability

Policy information about availability of computer code

Code availability statement

For all studies using custom code, the Methods section must include a statement under the heading "Code availability" describing how readers can access the code, including any access restrictions.

☐ A full code availability statement is included in the manuscript

Research animals

Policy information about studies involving animals; ARRIVE guidelines recommended for reporting animal research

Ethical compliance

☒ Confirm that you have complied with all relevant ethical regulations and that a statement affirming this is included in the manuscript.

Ethics committee

☒ Confirm that the manuscript states the name(s) of the board and institution that approved the study protocol.

I certify that all the above information is complete and correct.

Typed signature Robert E. Campbell Date November 20, 2018

nature methods

SUPPLEMENTARY INFORMATION

https://doi.org/10.1038/s41592-018-0294-6

In the format provided by the authors and unedited.

A genetically encoded near-infrared fluorescent calcium ion indicator

Yong Qian[1,12], Kiryl D. Piatkevich[2,12], Benedict Mc Larney[3,4,12], Ahmed S. Abdelfattah[5], Sohum Mehta[6], Mitchell H. Murdock[2], Sven Gottschalk[3], Rosana S. Molina[7], Wei Zhang[1], Yingche Chen[1], Jiahui Wu[1], Mikhail Drobizhev[7], Thomas E. Hughes[7], Jin Zhang[6], Eric R. Schreiter[5], Shy Shoham[8], Daniel Razansky[3,4,9,10], Edward S. Boyden[2] and Robert E. Campbell[1,11]*

[1]Department of Chemistry, University of Alberta, Edmonton, Alberta, Canada. [2]Media Lab and McGovern Institute for Brain Research, MIT, Cambridge, MA, USA. [3]Institute for Biological and Medical Imaging, Helmholtz Center Munich, Neuherberg, Germany. [4]Faculty of Medicine, Technical University of Munich, Munich, Germany. [5]Janelia Research Campus, Howard Hughes Medical Institute, Ashburn, VA, USA. [6]Department of Pharmacology, University of California San Diego, La Jolla, CA, USA. [7]Department of Cell Biology and Neuroscience, Montana State University, Bozeman, MT, USA. [8]Departments of Ophthalmology and of Neuroscience and Physiology, New York University Langone Health, New York City, NY, USA. [9]Faculty of Medicine and Institute of Pharmacology and Toxicology, University of Zurich, Zurich, Switzerland. [10]Department of Information Technology and Electrical Engineering and Institute for Biomedical Engineering, ETH Zurich, Zurich, Switzerland. [11]Department of Chemistry, Graduate School of Science, The University of Tokyo, Tokyo, Japan. [12]These authors contributed equally: Yong Qian, Kiryl D. Piatkevich, Benedict Mc Larney. *e-mail: robert.e.campbell@ualberta.ca

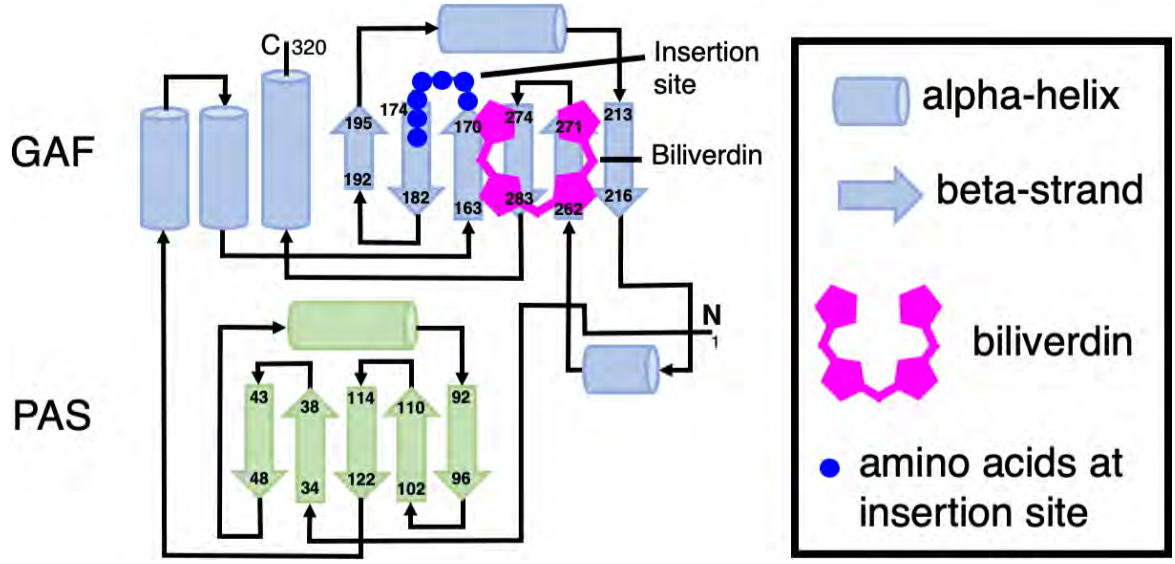

Supplementary Figure 1

The topology of mIFP (i.e., bacteriophytochrome).

Scheme is based on alignment of the sequence of mIFP (320 residues; GenBank accession number AKH03689.1; *Nat. Methods* **12,** 763–765, 2015), with the crystal structure of the chromophore-binding domain of *Deinococcus radiodurans* BphP (PDB 2O9B; *J. Biol. Chem.* **282,** 12298–12309, 2007). Representation is adapted from Takala et al. (*Nature* **509,** 245–248; 2014), with β-strands represented as arrows and α-helical regions represented as cylinders. The PAS domain is colored in light green, and the BV-binding GAF domain is colored in light blue, as in Fig. 1a,b. The approximate position of the bound BV is represented by a magenta structure. Numbers at the ends of β-strands correspond to mIFP numbering (see Supplementary Figs. 2c, 3 and 4), based on alignment with the crystal structure. To engineer NIR-GECO1, 5 residues (171–175, DEEGN) in the loop between the first two β-strands of the GAF domain were initially replaced with a 182-residue CaM-RS20 domain (a 3-residue linker followed by 147-residue CaM followed by a 5-residue linker followed by 23-residue RS20 followed by a 4-residue linker). Systematic optimization of the insertion site to improve the Ca^{2+}-dependent fluorescence change led to the deletion of residues 176G and 177E of mIFP, resulting in an overall replacement of 7 residues (171–177, DEEGNGE) with the CaM-RS20 domain.

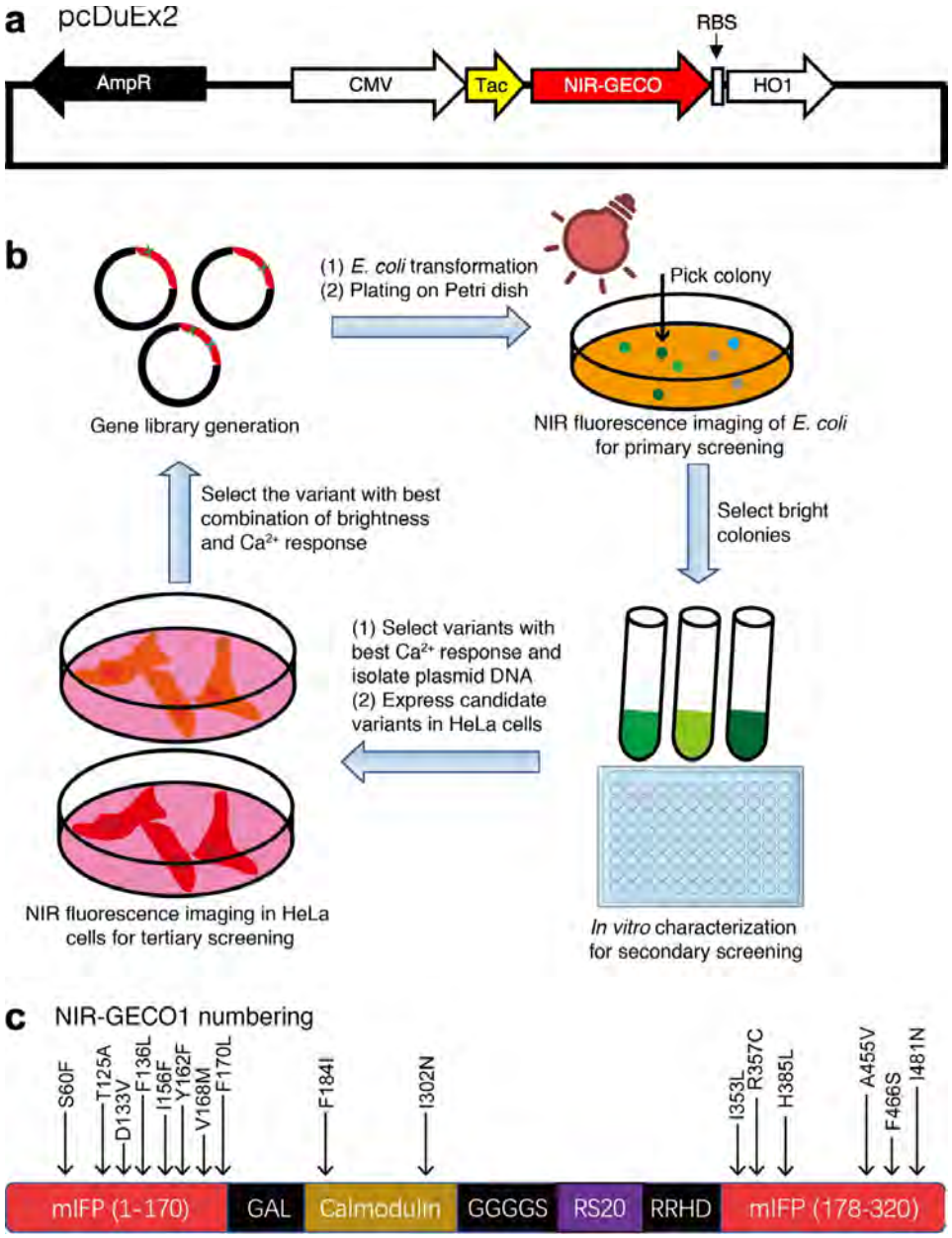

Supplementary Figure 2

Directed evolution of NIR-GECO1 by library screening.

(**a**) Representation of the pcDuEx2 vector used for expression of genes in both bacteria and mammalian cells. Cytomegalovirus (CMV) promoter is used for mammalian expression, while the *Tac* promotor (a hybrid promoter derived from the *trp* and *lac* promoters) is used for bacterial expression. HO1 is expressed in bacteria but, because of the presence of a stop codon after NIR-GECO1 and the lack of a promoter before HO1, it is not expressed in mammalian cells. RBS, ribosome binding site; HO1, heme-oxygenase 1. (**b**) Workflow of the screening process. Briefly, *E. coli* DH10B was transformed with a gene library in pcDuEx2 and grown on LB plates, and then bright colonies were picked and cultured. Proteins were extracted from overnight cultures of bacteria and then tested for fluorescence and Ca^{2+} response in 384-well plates. Variants with reasonable brightness and Ca^{2+} response were selected, and the corresponding plasmids were purified. HeLa cells were transfected with the selected plasmids, and live-cell fluorescence imaging was used to evaluate both brightness and Ca^{2+} response. HeLa cells were not supplemented with BV. (**c**) Mutations of NIR-GECO1 acquired during directed evolution.

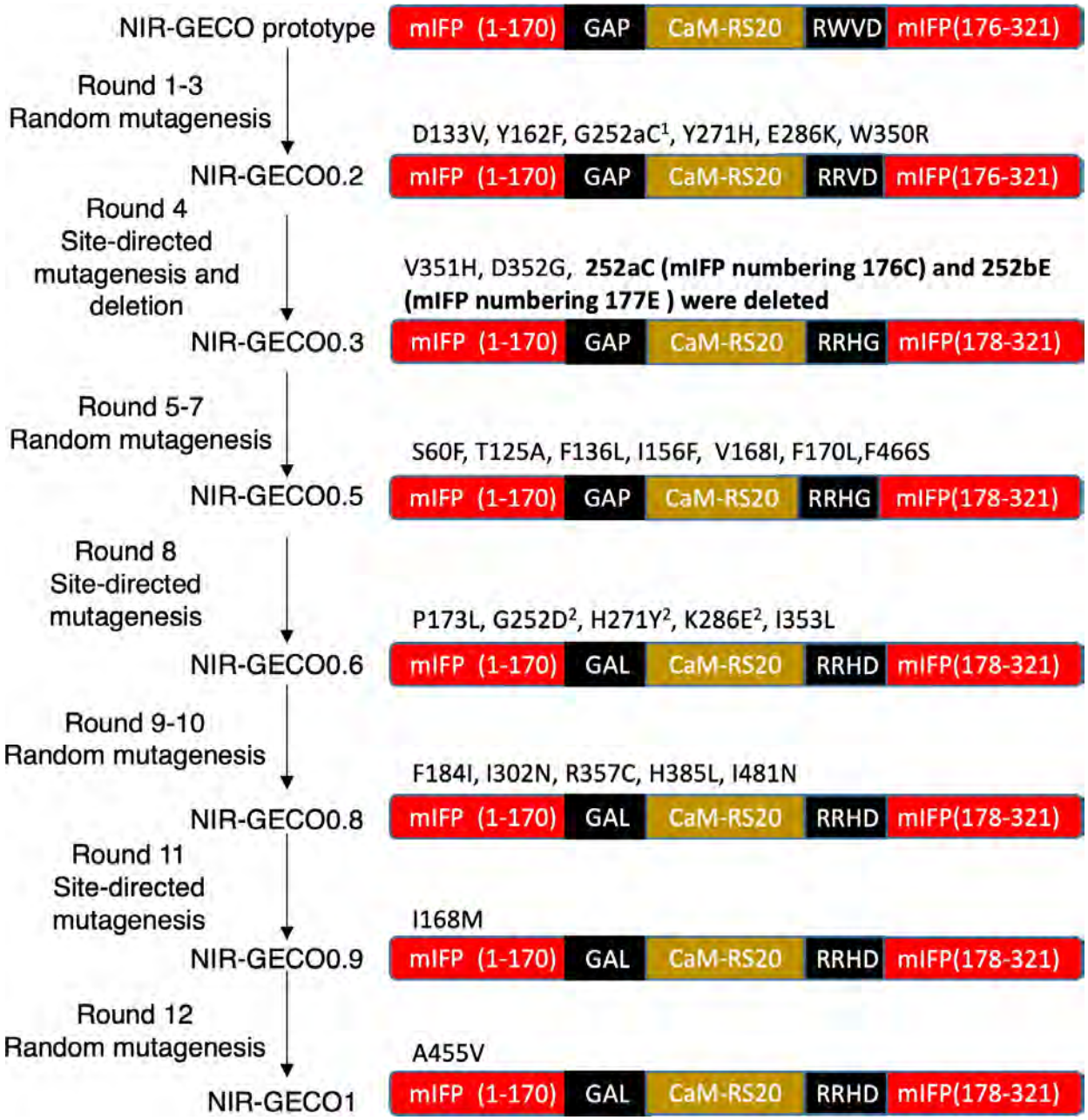

Supplementary Figure 3

Lineage of improved NIR-GECO variants.

Key mutations included deletion of 252aC and 252bE, which substantially improved the Ca^{2+}-dependent fluorescence change; F184I and I302N, which increased affinity for Ca^{2+}; and W350R and R357C, A455V which substantially improved the brightness. Footnotes: [1]This residue was deleted in round 4. [2]These mutations were reversions.

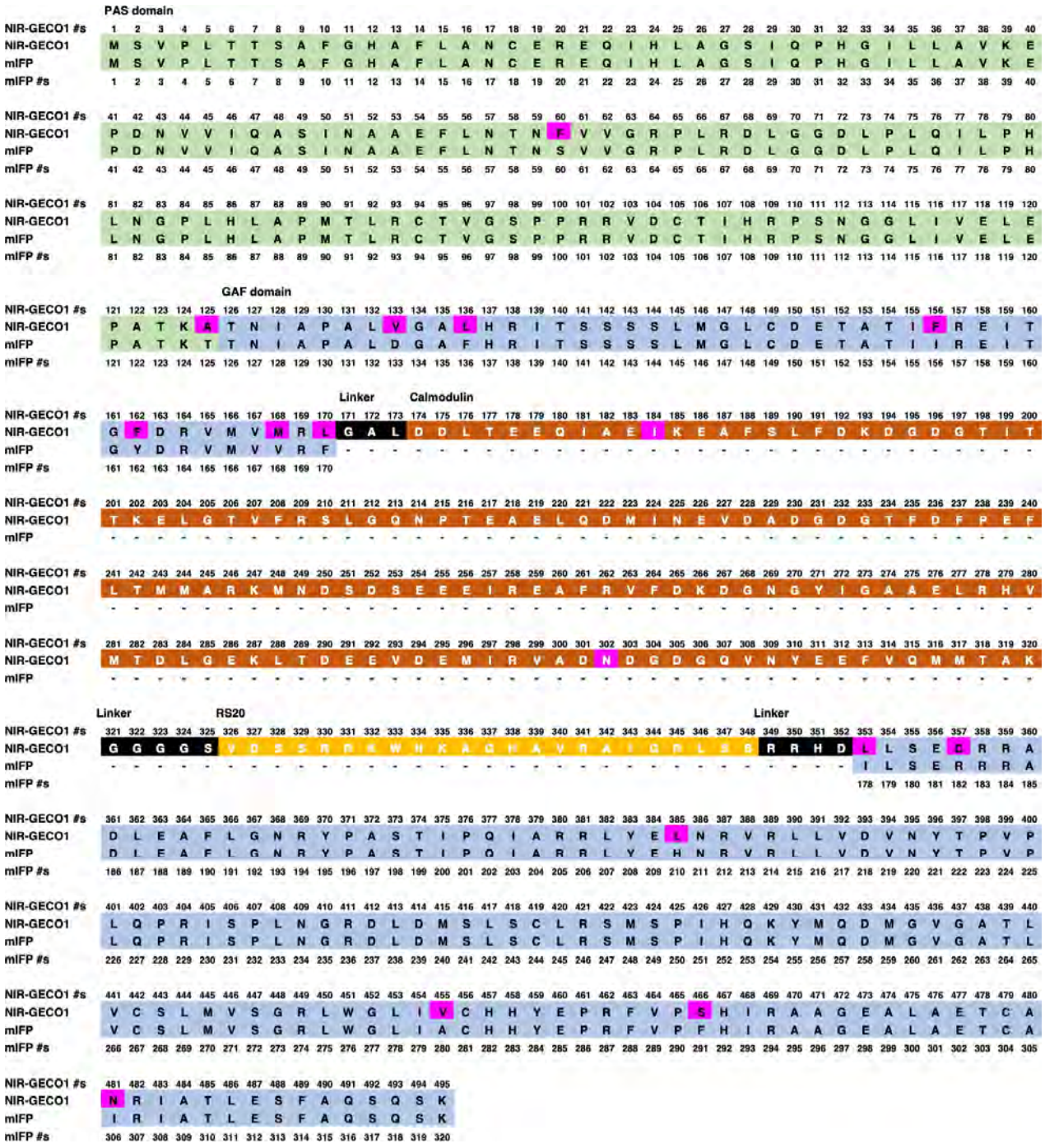

Supplementary Figure 4

Sequence alignment of NIR-GECO1 and mIFP.

Single-amino-acid changes relative to mIFP and calmodulin are highlighted with a magenta background. PAS domain, GAF domain, linkers, calmodulin, and RS20 are shown as light green, light blue, black, brown, and yellow, respectively, consistent with domain colors in Fig. 1a,b and Supplementary Fig. 1.

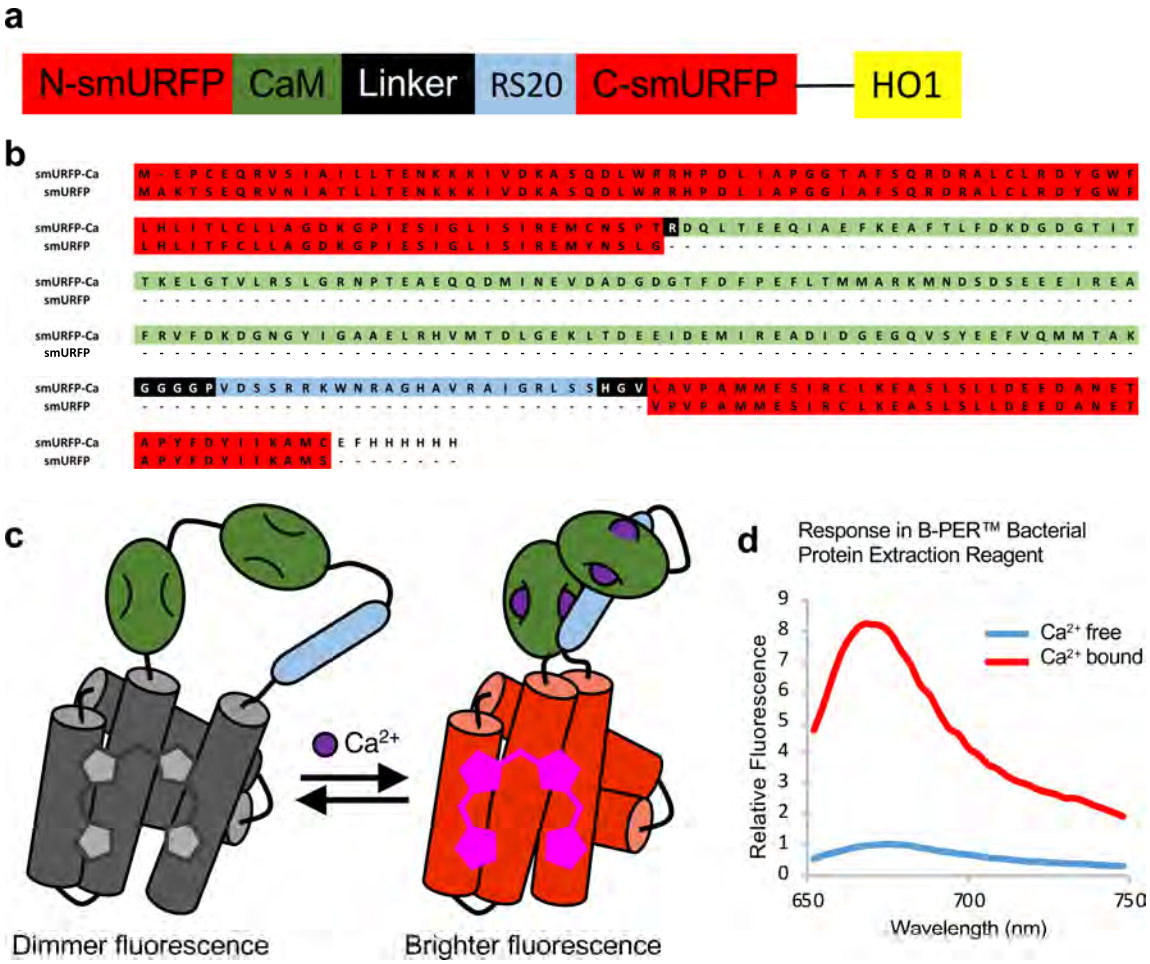

Supplementary Figure 5

Attempted engineering of a smURFP-based Ca^{2+} indicator.

Using methods analogous to those used to develop NIR-GECO1, we attempted to engineer a smURP-based (*Nat. Methods* **13,** 763-769; 2016) Ca^{2+} indicator. During each round of screening, the protein was tested for Ca^{2+}-dependent fluorescent response in crude bacterial lysate prepared with B-PER protein extraction reagent (Thermo Fisher). Under these conditions, this indicator exhibited a substantial fluorescence increase upon binding Ca^{2+}. Unfortunately we were unable to functionally express this indicator in mammalian cells. (**a**) Schematic representation of the smURFP-based Ca^{2+} indicator structure. (**b**) Sequence of the indicator after the eighth round of directed evolution. (**c**) Schematic representation of the protein structure and response. CaM-RS20 was inserted between the fourth and fifth helix of smURFP. The best variant exhibited an approximately eightfold change in fluorescence intensity (Ca^{2+}-bound/Ca^{2+}-free) at the maximum emission (670 nm). (**d**) Emission spectra for the protein after the eighth round, normalized to the Ca^{2+}-free state.

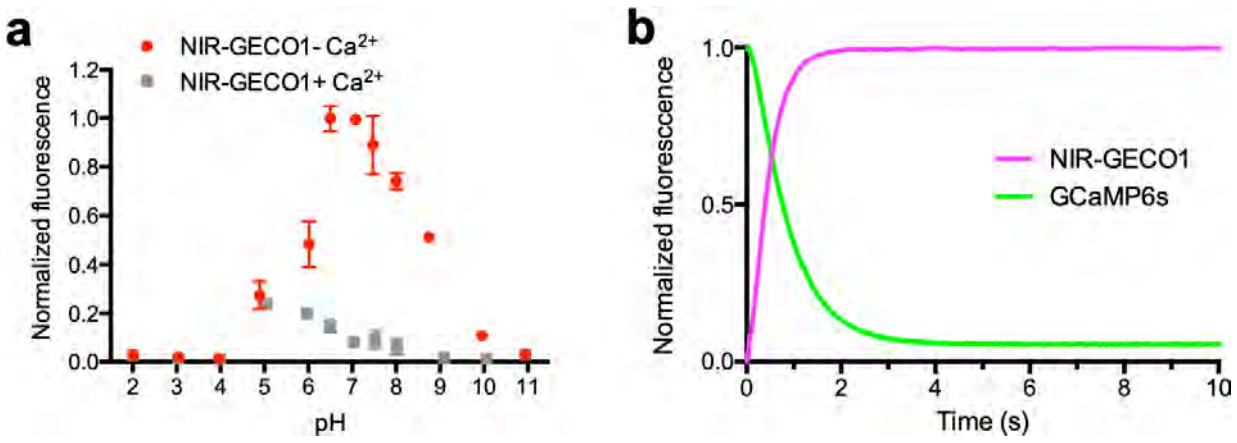

Supplementary Figure 6

Additional in vitro characterization of NIR-GECO1.

(**a**) pH titration curves of NIR-GECO1 in the presence and absence of Ca^{2+}. *n* = 3 independent experiments; values are mean ± s.d. (**b**) Ca^{2+} dissociation kinetics of NIR-GECO1 (magenta) and GCaMP6s (green).

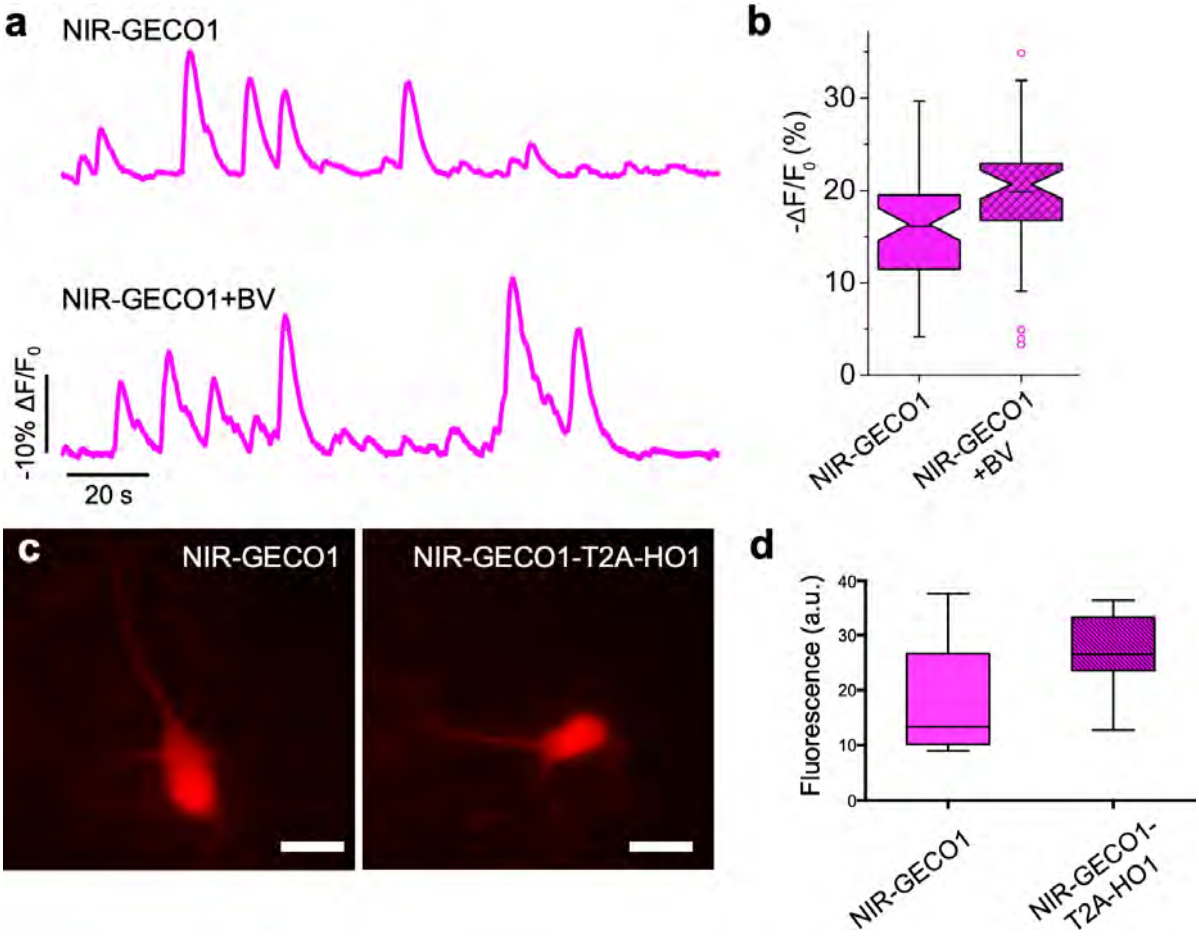

Supplementary Figure 7

Increasing intracellular BV concentration has a modest effect on NIR-GECO1 brightness.

(**a**) Representative fluorescence traces of NIR-GECO1 (top) and NIR-GECO1 supplied with 25 μM exogenous BV (bottom) in response to neuronal spontaneous activities. *n* = 51 neurons for NIR-GECO and *n* = 39 neurons for NIR-GECO1 + BV. (**b**) Quantification of $-\Delta F/F_0$ corresponding to the experiment of **a**. Values are 16 ± 6% for NIR-GECO1 and 20 ± 8% for NIR-GECO1 + BV (mean ± s.d.). (**c**) Representative wide-field fluorescence images of neurons expressing NIR-GECO1 (left) and NIR-GECO1-T2A-HO1 (right). The human HO1 gene was used. Scale bar, 20 μm. (**d**) Relative normalized fluorescence of NIR-GECO1 (*n* = 15 neurons) and NIR-GECO1-T2A-HO1 (*n* = 15 neurons). Values are 18.3 ± 10.2 (a.u.) for NIR-GECO1 and 27.1 ± 7.0 (a.u.) for NIR-GECO1-T2A-HO1 (mean ± s.d.). Fluorescence was normalized by coexpression of EGFP (NIR channel, 650/60 nm Ex and 720/60 nm Em; green channel, 490/15 nm Ex and 525/50 nm Em). Box plots are used where the top and bottom horizontal lines mark the 25th and 75th percentiles for the data; whiskers extend to the maximum and minimum for the data; and the black horizontal bar is the median.

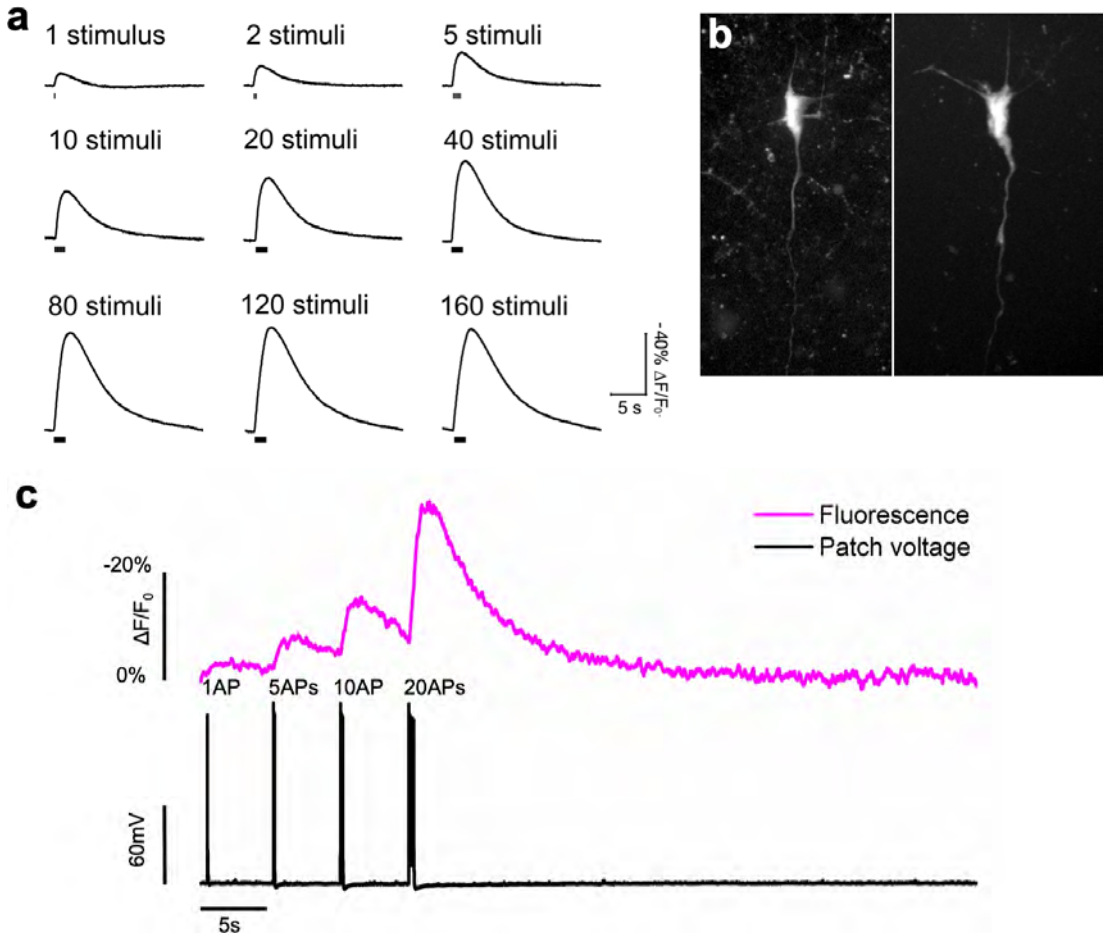

Supplementary Figure 8

Characterization of NIR-GECO1 in cultured neurons and in intact brain tissues.

(**a**) Representative traces of single trial NIR-GECO1 fluorescence responses to field stimulation in cultured rat hippocampal neurons. (**b**) Representative confocal images of neurons in L2/3 of motor cortex expressing NIR-GECO1 (641 nm Ex and 664LP Em; *n* = 4 slices from 2 mice). Such neurons were imaged during electrophysiological current injections as in **c**. (**c**) Representative single-trial wide-field optical recording of NIR-GECO1 fluorescence responses (magenta; 631/28 nm Ex and 664LP Em; acquisition rate 50 Hz) to 1, 5, 10, and 20 action potentials trains evoked by current injections in neurons in L2/3 of motor cortex (as in **b**; *n* = 6 neurons from 4 mice at P11-22). Patch voltage is shown in black.

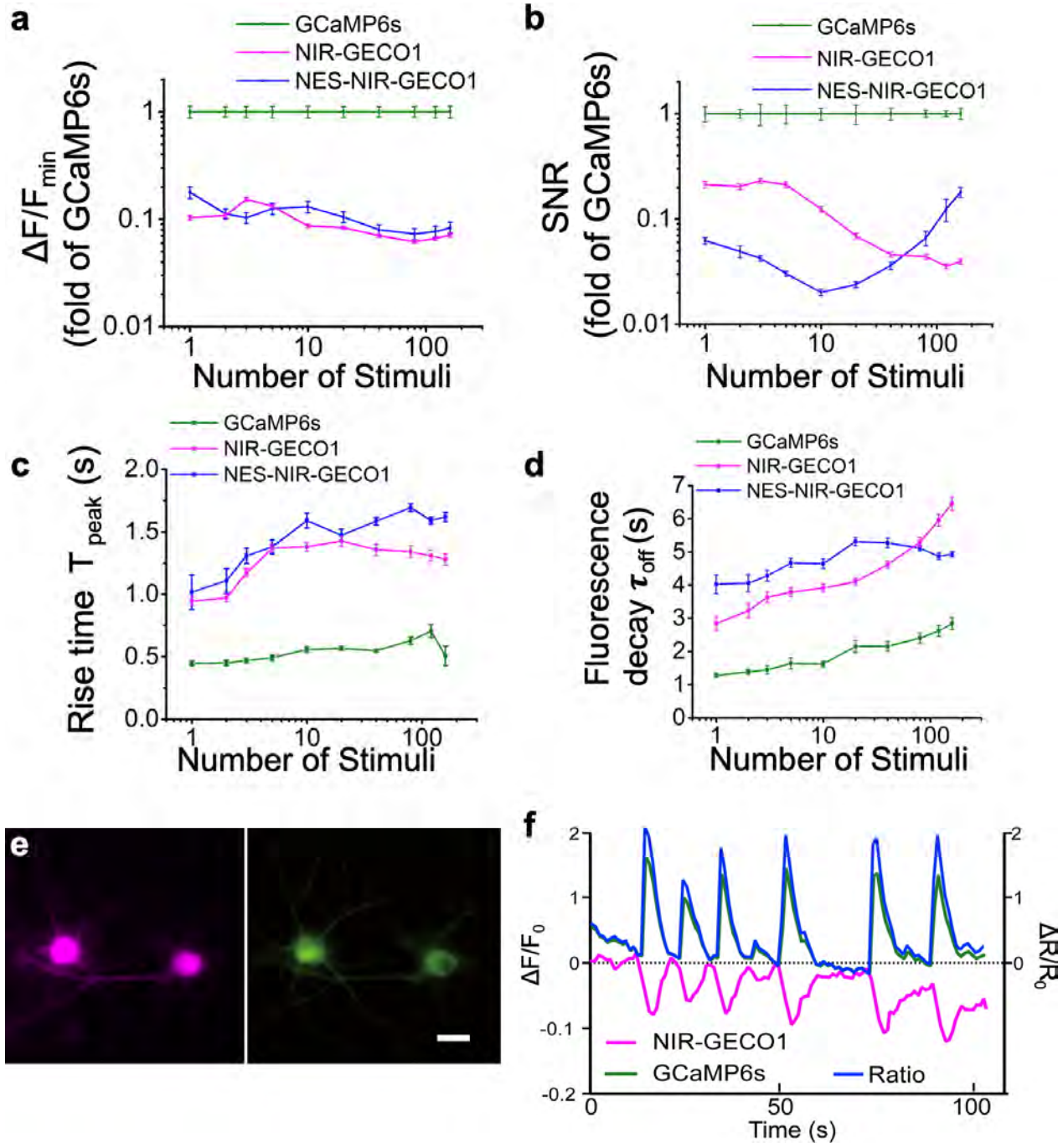

Supplementary Figure 9

Comparison of NIR-GECO1, NES-NIR-GECO1 and GCaMP6s.

(**a**) Response amplitude of NIR-GECO1 (n = 55 neurons) and NES-NIR-GECO1 (n = 147 neurons) as a fraction of GCaMP6s (n = 31 neurons). The average $-\Delta F/F_{min}$ of NIR-GECO1 was 2.4 ± 0.12%, 3.4 ± 0.16%, 6.6 ± 0.29%, 11 ± 0.44%, 17 ± 0.65%, 27 ± 0.9%, 43 ± 1.4%, 60 ± 2.0%, 77 ± 3.0%, and 94 ± 4.2% for 1, 2, 3, 5, 10, 20, 40, 80, 120 and 160 APs, respectively. Relative to GCaMP6s, the $-\Delta F/F_{min}$ of NIR-GECO1 was 10% of GCaMP6s for 1 and 2 APs and increased to 15% and 13% for 3 and 5 APs and then went down to 7% for APs from 10 to 160 APs. Elsewhere in the paper we have consistently used $\Delta F/F_0$ to describe fluorescence changes. Here we use $\Delta F/F_{min}$ to enable the values for NIR-GECO1 and GCaMP6s to be easily compared. (**b**) Signal-to-noise ratio (SNR) of NIR-GECO1 and NES-NIR-GECO1 compared to GCaMP6s. The SNR of NIR-GECO1 was 26.7 ± 1.98, 34.4 ± 2.15, 62.2 ± 3.42, 98.6 ± 6.37, 145 ±

9.29, 185 ± 10.9, 256 ± 15.3, 302 ± 18.0, 311 ± 16.9 and 335 ± 18.8 for 1, 2, 3, 5, 10, 20, 40, 80, 120 and 160 APs, respectively. Relative to GCaMP6s, the SNR of NIR-GECO1 was 20% of GCaMP6s for APs from 1 to 5 and then goes down to 12% to 4% of GCaMP6s for APs from 10 to 100. (**c**) Fluorescence rise time of NIR-GECO1 and NES-NIR-GECO1 (actually a fluorescence decrease) compared to GCaMP6s for binding of Ca^{2+}. The average rise time of NIR-GECO1 was 0.94 ± 0.033 s, 1.4 ± 0.038 s, 1.4 ± 0.044 s for 1, 10 and 40 APs. (**d**) Fluorescence decay time of NIR-GECO1 and NES-NIRGECO1 (actually a fluorescence increase) compared to GCaMP6s for dissociation of Ca^{2+}. The average decay time of NIR-GECO1 was 2.8 ± 0.21 s, 3.9 ± 0.12 s, 4.6 ± 0.11 s for 1, 10 and 40 APs. For **a**–**d**, the NIR-GECO1 data are identical to data represented in Fig. 1i–l. For **a**–**d**, center values are the mean, and error bars are s.e.m. *n* = 55 neurons for NIR-GECO1 and *n* = 31 neurons for GCaMP6s. (**e**) Representative wide-field fluorescence images of coexpressed NIR-GECO1 (left) and GCaMP6s (right). *n* = 5 neurons from two cultures. Scale bar, 20 μm. (**f**) Spontaneous Ca^{2+} oscillations in dissociated cortical neurons coexpressing NIR-GECO1 and GCaMP6s (NIR channel, 650/60 nm Ex and 720/60 nm Em; green channel, 490/15 nm Ex and 525/50 nm Em; acquisition rate is 1 Hz). Also shown is $\Delta R/R_0$, where R is the normalized GCaMP6s intensity divided by normalized NIR-GECO1 intensity. *n* = 5 neurons from two cultures.

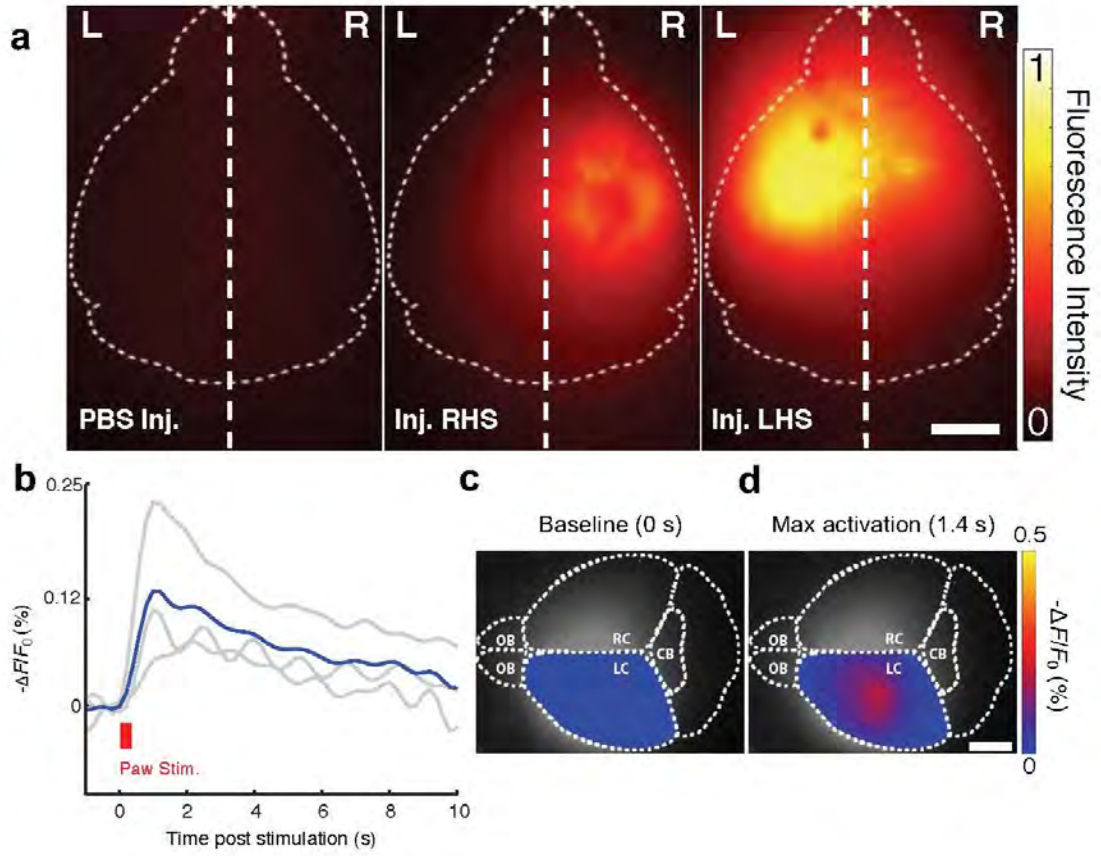

Supplementary Figure 10

In vivo mesoscale imaging of footshock responses in mice using NIR-GECO1.

(**a**) Mesoscale fluorescence images (671 nm Ex and 721/42 nm Em) of the mouse sensorimotor cortex injected with AAV2/9-hSyn1-NIR-GECO1 (as in Fig. 2e–g). Left, negative control with no viral expression on the right side of mouse brain (PBS injection). Middle, viral expression of NIR-GECO1 on the right side of mouse brain. Right, viral expression of NIR-GECO1 on the left side of mouse brain. Scale bar, 2 mm. (**b**) Fluorescence response of NIR-GECO1 in response to a paw stimulation paradigm with a single 50-ms pulse (0.5 mA). As in Fig. 2e, each gray line represents the averaged response of a mouse across 19 cycles, and the blue line represents the mean response from all 3 mice (n = 3, or 3 × 19 = 57 cycles). (**c**) Activation map of mouse brain before stimulation. The estimated brain outline was manually superimposed onto the fluorescence images to facilitate determining the site of injection and activation in relation to bregma and the sensorimotor cortex. (**d**) Activation map of mouse brain at max activation. Scale bar, 2 mm. OB, olfactory bulb; CB,

cerebellum; L/RC, left or right cortex.

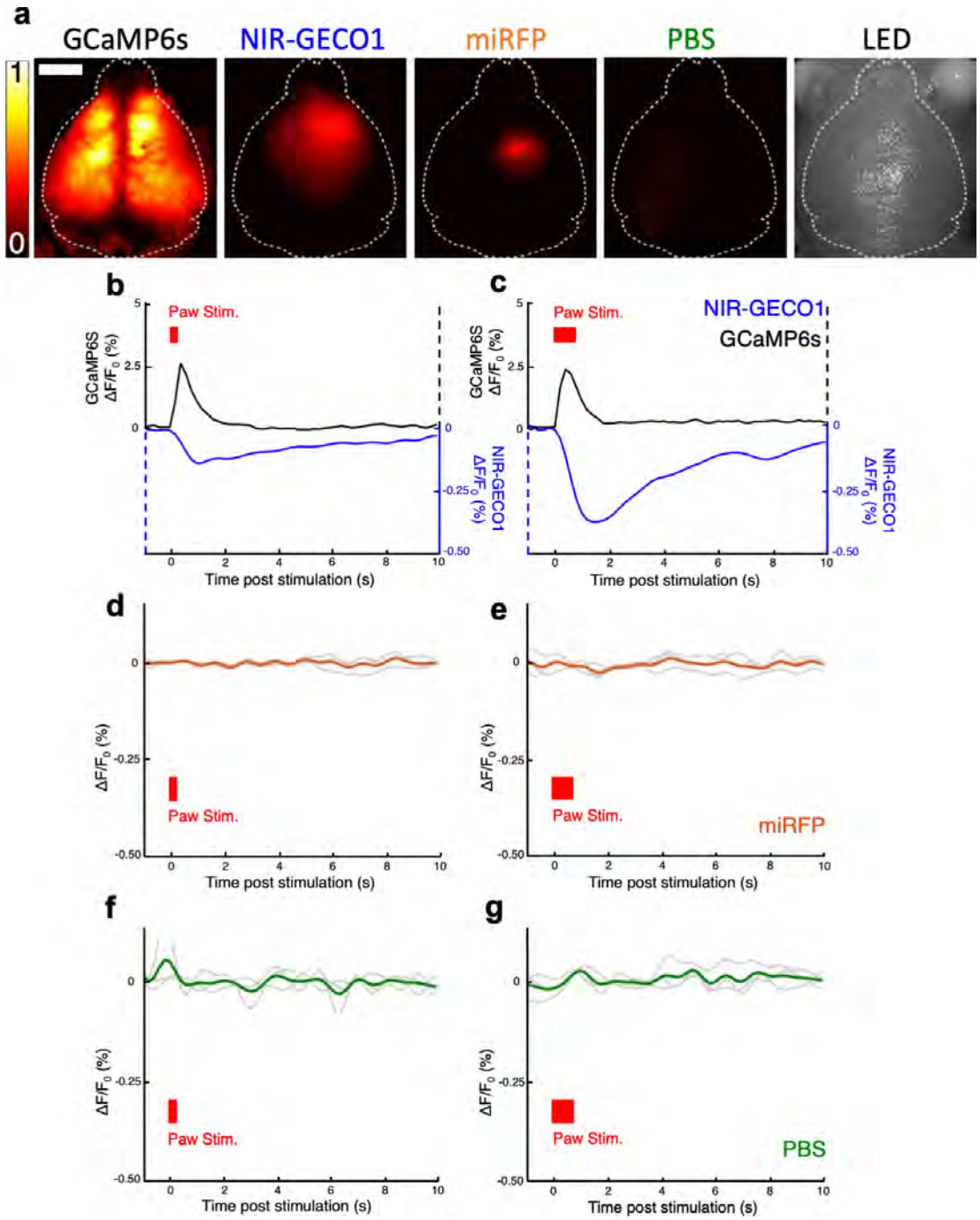

Supplementary Figure 11

Control experiments for in vivo mesoscale imaging using GCaMP6s and miRFP.

(a) Comparative fluorescence images of a transgenic Bl6-GCaMP6s mouse and FoxN1 nude NIR-GECO1, miRFP and PBS injected mice. All fluorescence images are normalized to the GCaMP image shown. Direct comparison of the NIR-GECO1 and miRFP brightness is complicated by the fact that the AAVs were different serotypes (AAV2/9 and AAV2, respectively) and the NIR-GECO1 stock had 10× more genome copies/mL. Also shown is a representative white light image of the imaging area. Scale bar, 2 mm. (**b, c**) Positive control experiment with imaging of GCaMP6s in response to paw stimulations. For **b**, a stimulation paradigm of a single 50-ms pulse (0.5 mA) was used. For **c**, a stimulation paradigm of 10 pulses in 700 ms (0.5 mA, 20 ms on and 50 ms off) was used. The mean

value from 3 mice is shown in each case. NIR-GECO1 curves are the same as in Supplementary Fig. 10b and Fig. 2e. (**d, e**) A negative control experiment with imaging of miRFP fluorescence in response to paw stimulations. Stimulations in **d** and **e** are the same as in **b** and **c**, respectively. Orange line represents the mean value from 3 mice, and gray lines represent the average response of 1 mouse across 19 cycles. (**f, g**) A negative control with fluorescence imaging PBS-injected mouse in response to paw stimulations. Filter set is the same as for NIR-GECO1. The green line represents the mean value of 3 measurements (an average of 19 cycles) from 2 mice, and the gray lines represent the average response averaged for 1 mouse measured once and 1 mouse measured twice. Stimulations in **f** and **g** are the same as in **b** and **c**, respectively. The GCaMP6s mice are a transgenic line, and the mice were approximately 2 months older than other mice used in these experiments.

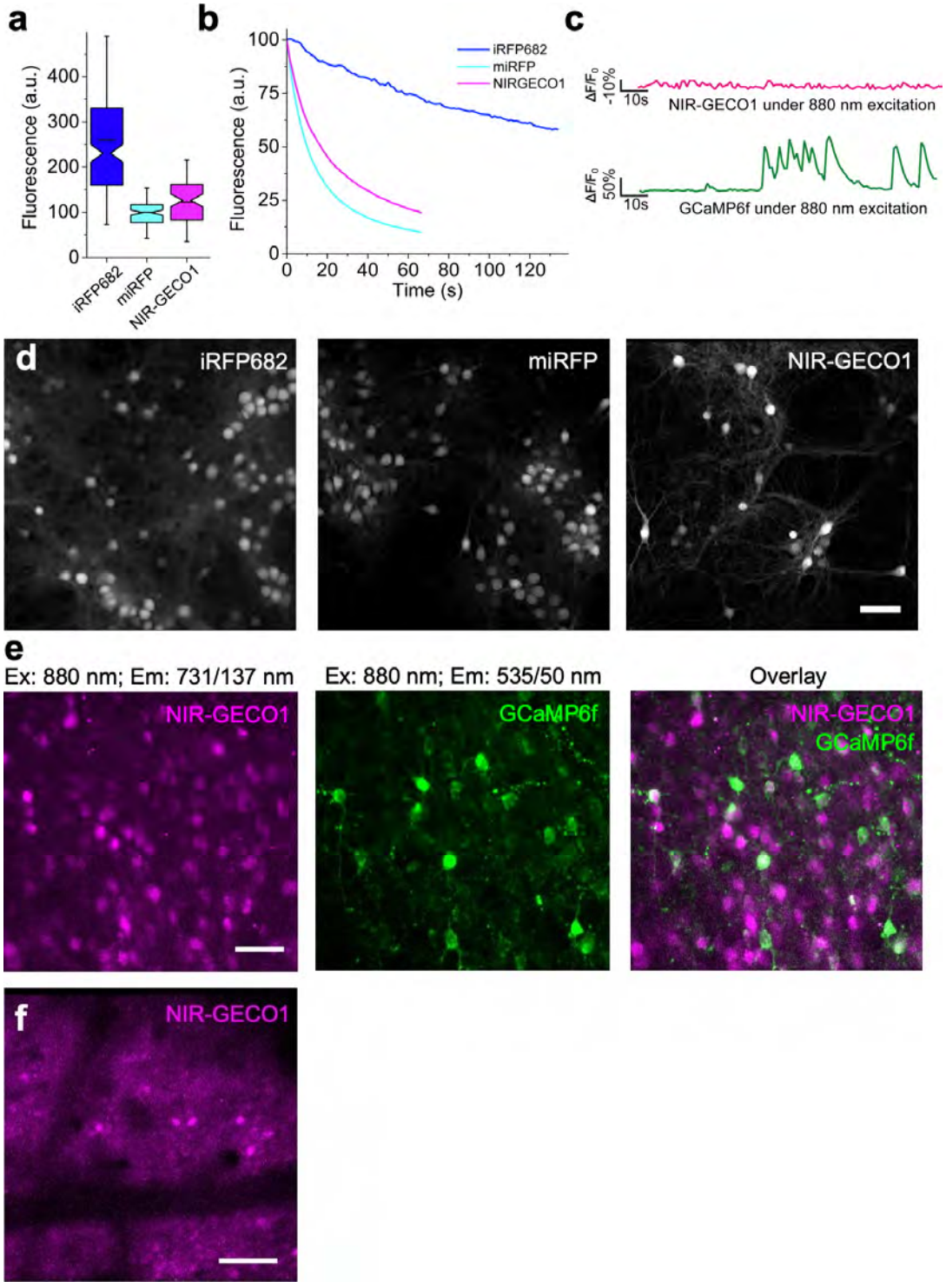

Supplementary Figure 12

Two-photon fluorescence microscopy of NIR-GECO1.

BV-FPs can be visualized using two-photon fluorescence microscopy (*Biophys. J.* **113,** 2299–2309; 2017), a widely used technique for *in vivo* Ca^{2+} imaging. (**a**) Relative normalized fluorescence and (**b**) raw photobleaching curves for iRFP682 (blue), miRFP (cyan), and

NIR-GECO1 (magenta) in cultured mouse neurons (*n* = 184, 106, and 77 cells, respectively, from one culture) under 880-nm two-photon excitation and 4.05 mW of total light power. For **a**, a box plot with notches is used as described in Fig. 1g. (**c**) Representative fluorescence recording of 4-aminopyridine (1 mM final concentration)-evoked neuronal activity using NIR-GECO1 and GCaMP6f fluorescence under 880-nm two-photon excitation. Excitation for both NIR-GECO1 and GCaMP6f was 880 nm, and emission filters for NIR-GECO1 and GCaMP6s were 705/90 nm and 518/45 nm, respectively. (**d**) Representative two-photon fluorescence images of cultured mouse neurons expressing iRFP682 (left), miRFP (middle) and NIR-GECO1 (right), under 880-nm two-photon excitation (731/137 nm Em; *n* = 184, 106, and 77 cells, respectively, from one culture). Scale bar, 50 μm. (**e**) Two-photon fluorescence images of live mouse brain slice coexpressing NIR-GECO1 (left; magenta) and GCaMP6s (middle; green) under 880-nm excitation (right, overlay). *n* = 2 slices from one mouse. Scale bar, 50 μm. (**f**) In vivo two-photon microscopy of NIR-GECO1-expressing neurons in mouse primary visual cortex. *n* = 3 fields of view from one mouse. Scale bar, 50 μm.

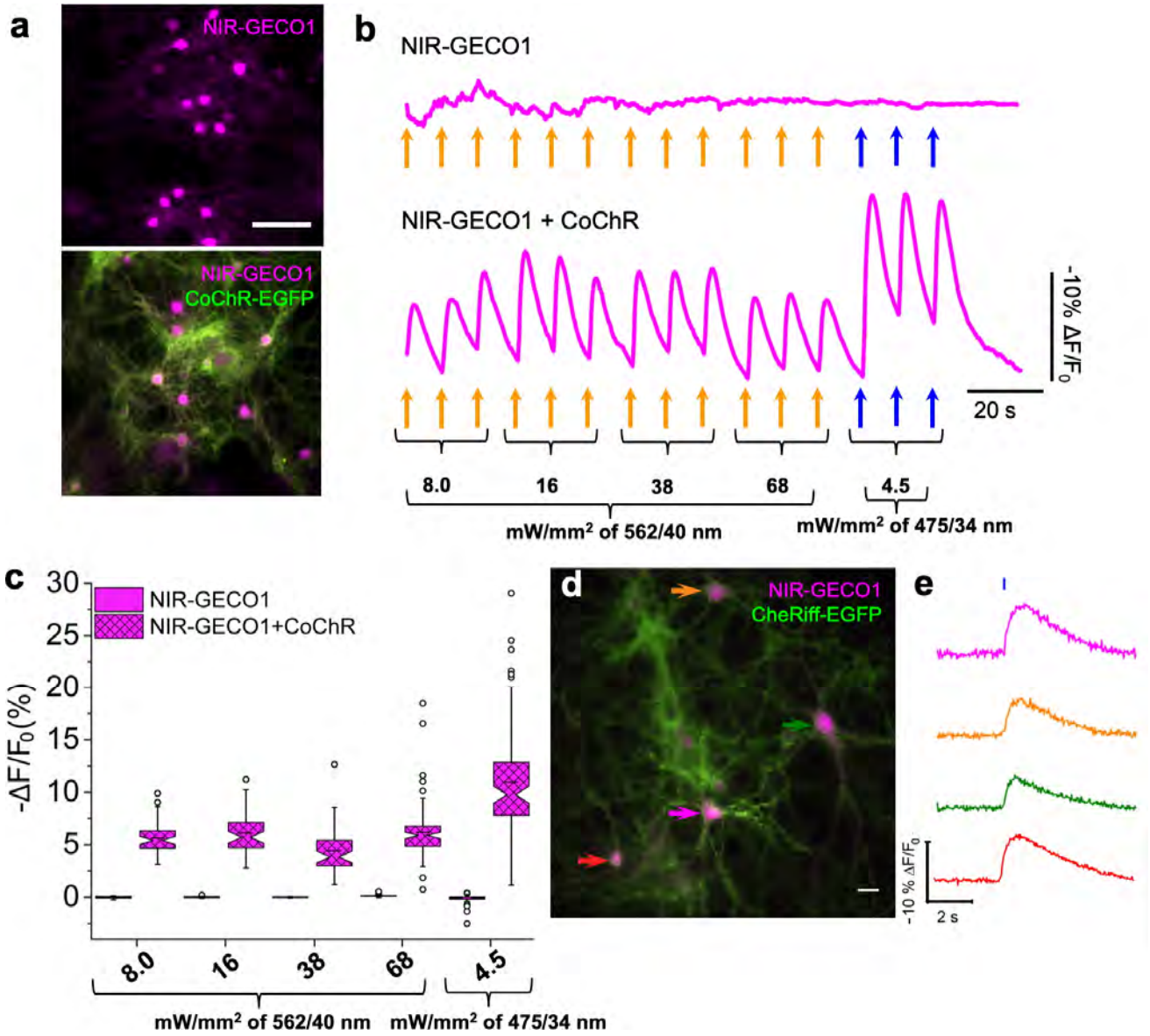

Supplementary Figure 13

Combined use of channelrhodopsins (CoChR and CheRiff) and NIR-GECO1 for optogenetic stimulation and imaging of activity.

Representative wide-field fluorescent images of cultured hippocampal mouse neurons expressing NIR-GECO1 (top; magenta; 631/28 nm Ex and 664LP Em), and both NIR-GECO1 (magenta; 631/28 nm Ex and 664LP Em) and CoChR-EGFP (*Nat. Methods* **11,** 338–346, 2014; *Nat. Neurosci.* **20,** 1796–1806, 2017) (green; bottom; 475/34 nm Ex and 525/50 nm Em). Scale bar, 50 µm. (**b**) Representative single trial traces for single neurons (as in **a**; *n* = 45 and 93 neurons for NIR-GECO1 and NIR-GECO1 + CoChR-EGFP, respectively, from two cultures) illuminated with 562/40 nm (orange arrows) or 475/34 nm (blue arrows) at indicated light intensities with 200-ms duration per pulse. (**c**) Quantification of NIR-GECO1 fluorescence changes in response to activation of CoChR under the conditions described in **b** (*n* = 45 and 93 neurons for NIR-GECO1 and NIR-GECO1 + CoChR-EGFP, respectively, from 2 cultures). Box plots with notches are used as described in Fig. 1g. (**d**) Image of cultured rat hippocampal neurons expressing CheRiff-EGFP (*Nat. Methods* **11,** 825–833; 2014) (green, 480 nm Ex and 525/36 nm Em) and NIR-GECO1 (magenta, 640 nm Ex and 705/50 nm Em). CheRiff is localized to the plasma membrane, whereas NIR-GECO1 fills the cytoplasm and nucleus of the neurons. Scale bar, 20 µm. (**e**) NIR-GECO1 fluorescence traces from 4 neurons, indicated with correspondingly colored arrows in **d**, in response to optical stimulation. Blue bar indicates a 10-ms blue light (490/20 nm at 4 mW/mm^2) illumination.

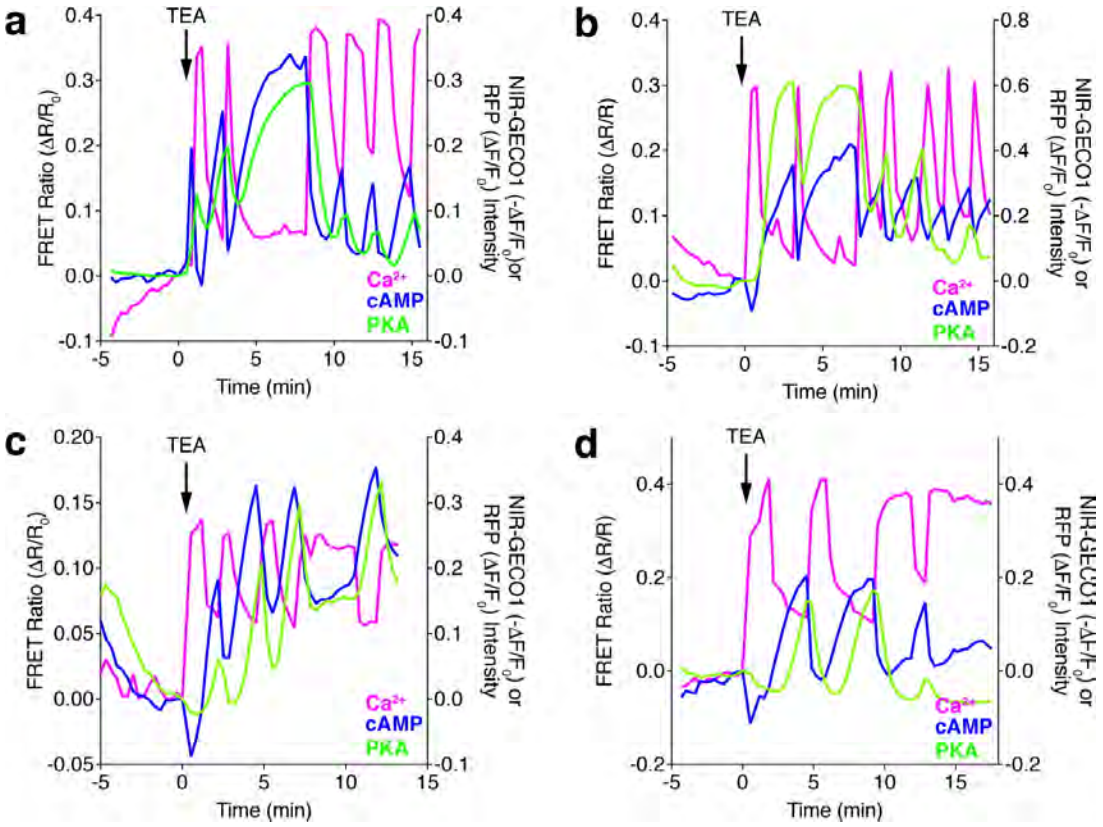

Supplementary Figure 14

Additional representative single-cell traces for multiplexed imaging of MIN6 β-cells.

Conditions are identical to those described for Fig. 3g. A video of the cell shown in panel **d** is provided as Supplementary Video 3.

Supplementary Table 1. Spectral, photochemical and biochemical properties of NIR-GECO1 in comparison with iRFP682 ,miRFP, GCaMP6s and GCaMP3.

Protein	$[Ca^{2+}]$ (mM)	Ex (nm)	Em (nm)	EC ($\times 10^3$ $mM^{-1}cm^{-1}$)	QY (%)	Photostability $t_{1/2}$[a] (s)	pK_a	Dynamic range[b]	Hill coeff. (n)	K_d (nM)	k_{off} (s^{-1})
NIR-GECO1	0[c]	678	704	62	6.3	480	6.03	8×	1.03	215	1.93
	5	678	704	20	1.9		4.68				
iRFP682[d]	N/A	670	682	69	11.3	1860[e]	4.6	N/A	N/A	N/A	N/A
miRFP[d]	N/A	674	703	92	9.7	2040[e]	4.3	N/A	N/A	N/A	N/A
GCaMP6s	0[c]	498	515	4.5	ND	ND	9.77	30×	2.4	144[f]	1.08
	5	498	512	73.4	61		6.00				
GCaMP3[g]	0[c]	496	513	ND	ND	ND	8.40	13×	2.1	405	ND
	1	496	513	37.0	65		6.97				

Abbreviations: Ex, fluorescence excitation maximum; Em, fluorescence emission maximum; EC, extinction coefficient; QY, quantum yield; $t_{1/2}$, half-time; pK_a, pH corresponding to 50% of the maximal fluorescence brightness measured at optimal pH; K_d, K_d for Ca^{2+}; k_{off}, Ca^{2+}-dissociation kinetics measured by stopped-flow spectrometer; N/A, not applicable. ND, not determined.

[a]Measured in cultured neurons under continuous 631/28 nm wide-field illumination at 38 mW/mm^2.

[b]F (zero free Ca^{2+})/F (~39 μM free Ca^{2+}) for NIR-GECO1 and F (~39 μM free Ca^{2+})/F (zero free Ca^{2+}) for GCaMP6s. NIR-GECO1 is not completely saturated in 39 μM free Ca^{2+}. The value of F (zero free Ca^{2+}) /F (5 mM Ca^{2+}) is 10.6.

[c]In presence of 10 mM EGTA (zero free Ca^{2+}).

[d]Data from Ref. 1.

[e]Extrapolated using the data shown in **Fig. 1h**.

[f]Data from Ref. 2,3.

[g]Data from Ref. 4.

Supplementary Note 1: **Rationale for a non-permutated indicator topology.**

The primary challenge of designing a single FP-based GECI is to engineer an allosteric connection between a Ca^{2+}-dependent conformational change (e.g., by calmodulin (CaM)[5], interaction of CaM and a Ca^{2+}-CaM-binding peptide (CBP)[2,6], or troponin C (TnC)[7]), into a change in the FP fluorescence. Achieving this goal requires that the Ca^{2+}-binding domain be in close proximity to the FP chromophore, whether it is the autogenically synthesized chromophore of a β-FP, or the bound BV of a BV-FP. In the case of β-FPs, this has been achieved by either fusing CaM and the CBP to the termini of the protein that has been circularly permutated such that the termini are in close proximity to the chromophore[2,6], or by directly inserting the Ca^{2+}-binding domain into β-FP at a position close to the chromophore[5,7]. Single FP-based Ca^{2+} indicators with both circularly permutated (i.e., Ca^{2+}-sensing domains fused to the termini of a circularly permutated FP) and non-circularly permuted (i.e., a Ca^{2+}-sensing domain inserted into an FP) topologies have been reported. Examples of circularly permutated indicators include GCaMP[2,3], Pericam[6], R-GECO1 (Ref. 8), RCaMP1 (Ref. 9), and K-GECO1 (Ref. 10) and derivatives thereof[11–15]. There are fewer examples to date of non-circularly permutated indicators, with camgaroo[5] and NTnC[7] serving as prototypical examples.

While the apparent success of the circularly permutated design suggests that it would be a good basis for designing a BV-FP GECI, we chose to pursue a non-circularly permutated design based on Ca^{2+}-binding domain insertion. There were two reasons for choosing this design. The first reason is that we have found that some circularly permutated indicators can be converted to non-permutated topologies, with minimal impact on their function. For example, non-circularly permutated iGluSnFR (G^{ncp}-iGluSnFR) retains a fluorescence response and glutamate affinity that is very similar to iGluSnFR[16]. The second reason is that the N- and C-termini of BV-FPs are ~33 Å from each other (vs. ~ 24 Å for GFP) suggesting that a particularly long linker would be required to join the termini in a circularly permutated variant.

We suspect that the non-circularly permutated topology, in which the critical, and biologically promiscuous, CaM domain is genetically linked at both termini, may have two key advantages relative to a circularly permuted (i.e., GCaMP-type) topology. In a circularly permuted topology, the CaM is fused at one terminus and thus may be more accessible for interaction with endogenous protein binding partners leading to perturbations of normal cell biology. The first advantage is that the non-circularly permutated topology leaves the original N- and C-termini of

the FP available for genetic fusion to other proteins of interest or targeting motifs. In contrast to the circularly permutated topology, where the N- and C-termini are associated with RS20 and CaM, respectively, fusion to the normal FP termini is less likely to adversely affect the performance of the indicator itself.

Supplementary Note 2: Methods for two-photon spectral measurements.

Two-photon spectra and cross sections were measured using femtosecond excitation of fluorescence relative to known standards. The optical setup consists of a tunable femtosecond laser (DeepSee, InSight) coupled with a PC1 ISS fluorometer operating in photon-counting mode. The sample solution was continuously stirred in a 1 cm cuvette (Starna), and the laser beam was focused onto the sample with an achromatic lens (f = 60 mm, Qioptiq) close to the edge of the cuvette (~1 mm) to minimize the effects of solvent absorption. LDS798 (Exciton) in slightly alkaline $CDCl_3$ was used to correct for the two-photon spectral shape[17]. LDS798 in $CHCl_3$ served as the standard for two-photon cross section measurements[17]. Fluorescence of both the sample and the standard was excited at 1000 nm and recorded with the PC1 ISS monochromator at 720 nm. To eliminate possible errors resulting from independent measurements of the ECs and optical densities of dilute solutions, the Strickler-Berg approach was used to calculate the cross sections, using Equation 9 in the Supplementary Information of Ref. 18. This approach relies on the fluorescence lifetime (τ) of the sample and the QY and EC of the two-photon standard (LDS798 in $CHCl_3$, EC = 41,000 $M^{-1}cm^{-1}$)[17]. Rose Bengal (Sigma Aldrich) in MeOH served as a lifetime standard (τ = 0.519 ns)[19]. The fluorescence lifetimes of the samples were measured with the digital frequency domain technique (ChronosDFD, ISS) implemented with the PC1 ISS fluorometer (NIR-GECO1 Ca^{2+}-saturated τ = 0.48 ns, Ca^{2+}-free τ = 0.42 ns). Fluorescence was excited at 450 nm with a diode laser and recorded through a 700/13 bandpass filter. The fluorescence QY of LDS798 in $CHCl_3$ was measured with an integrating sphere (Quantaurus-QY Absolute PL quantum yield spectrometer, Hamamatsu) (QY = 0.16; 640 nm Ex).

As shown in **Fig. 3a**, two-photon absorbance spectrum of NIR-GECO1 is similar to that of other iRFPs[20]. That is, the cross-sectional value for the Soret band at <950 nm (50-75 GM) is substantially larger than for the Q band at ~1255 nm (<27 GM)

Supplementary Note 3: Methods for *in vivo* two-photon microscopy.

AAV injection protocol. For two-photon *in vivo* imaging for **Supplementary Fig. 12f** we expressed NIR-GECO1 in the mouse cortex via AAV and installed a chronic head plate with optical window above the corresponding brain area. Anesthesia was induced using isoflurane (induction, 3%; maintenance, 1-2%). We administered meloxicam (2 mg/kg i.p.) and slow-release buprenorphine (1 mg/kg) as analgesics. After animals were placed in a stereotaxic frame (Kopf Instruments), sterile eye lubricant (Puralube, Fisher Scientific) was administered to prevent corneal drying, and a heating pad was used to maintain body temperature. The scalp was opened using a midline incision, and the region to be imaged (primary visual cortex) was identified using stereotaxic coordinates (2.5 mm anterior to bregma, 2.55 mm lateral from the midline). A small craniotomy was opened in the skull using a 0.5-mm burr (Fine Science Tools) and a high-speed hand dental drill. The AAV (AAV2/9-hSyn1-NIR-GECO1, 500 nL) was injected 200 μm beneath the surface of the brain at a rate of 150 nL/min using a Nanofil syringe (World Precision Instruments) with a 33 G beveled needle (World Precision Instruments) and pump (World Precision Instruments). After the injection, the needle was kept in place for two minutes to allow time for diffusion of the virus prior to removing the needle from the brain. The scalp was closed using Vetbond.

Cranial window surgery. We allowed animals to recover from AAV injection surgeries before placing cranial windows. Anesthesia was induced using isoflurane (induction, 3%; maintenance, 1-2%). We administered meloxicam (2 mg/kg i.p.) and slow-release buprenorphine (1 mg/kg) as analgesics. After animals were placed in a stereotaxic frame (Kopf Instruments), sterile eye lubricant (Puralube, Fisher Scientific) was administered to prevent corneal drying, and a heating pad was used to maintain body temperature. Scalp fur was trimmed and a small circular section of skin (~1 cm in diameter) was excised using surgical scissors (Fine Science Tools). The periosteum was removed using fine forceps (Fine Science Tools). A custom-made circular head plate was attached to the skull using dental cement (C&B Metabond, Parkell Inc.) and centered around the region to be imaged. The head plate was then screwed into a custom-built fork fixed to a solid metal base.

Under a continuous gentle flow of phosphate-buffered saline (137 mM NaCl, 27 mM KCl, 10 mM phosphate buffer), a ~4-mm circular section of the skull, slightly larger than the window and centered over the injection site, was removed using a 0.5-mm burr (Fine Science Tools) and a high-speed hand dental drill, taking great care not to compress brain tissue or damage the

underlying vasculature. Sterile sugi swabs (John Weiss & Son, Ltd) were used to absorb trace bleeding. A 3-mm glass coverslip (Warner Instruments) was gently placed over the brain. Veterinary adhesive (Vetbond, Fisher Scientific) was used to form a seal between the coverslip and the skull. A layer of Metabond was then applied for added durability. Meloxicam (2 mg/kg i.p.) was administered as an analgesic 24 hours after surgery, and as needed thereafter. After allowing two weeks for expression, we imaged NIR-GECO1 in anesthetized, head-fixed mice using the two-photon microscope described in **Online Methods**.

Supplementary Note 4: Methods for *in vivo* mesoscale imaging.

AAV injection protocol. Four-week-old athymic female nude mice (Envigo, New Jersey, USA; stock number *Foxn1*^{nu}069) were injected with one of the following: 3 µL of AAV2/9-hSYN1-NIR-GECO1 virus at a concentration of 10^{13} genome copies/mL (Neurophotonics Centre, Université Laval, Canada); 3 µL of AAV2-hSyn1-miRFP virus at a concentration of 10^{12} genome copies/mL (UNC Vector core facility); or 3 µL of Dulbecco's Phosphate Buffered Saline solution (PBS) (D8357, Sigma-Aldrich, Taufkirchen, Germany). For analgesia, mice were administered a single oral drop of a 125 mg/mL Metamizole solution (Novalgin®, Sanofi-Aventis Deutschland GmbH, Frankfurt am Main, Germany) directly before and 4 hours after the injection. Anesthesia was induced via isoflurane (Isothesia®, Henry Schein®, NY, USA) at 3% v/v in 100% O_2. The mouse was placed into a custom head holder (SGM-4, Narishige International Limited, London, United Kingdom) connected to an anesthesia unit (Sigma Delta Vaporize, Penlon, UK). This head holder employs three points of fixation to hold the head in place: the incisors are placed into an opening in the metal holder, an anesthesia mask then covers the nose and an ear bar is placed into respective ears. Fixation in this way allows for easy access to the top of the head whilst allowing adjustment of head height, tilt and rotation. All of this is achieved without the need for implantation of external components on the skull of the mouse[21]. Once correctly positioned, a small incision was made down the middle of the scalp using a scalpel. Both sides of the scalp were pulled aside to allow access to the skull. Hemostatic sponges (Gelfoam®, Pfizer Pharmaceutical, NY, USA) were used to contain any bleeding during the procedure. A hole approximately 1 mm in diameter was carefully drilled into the skull, above the primary somatosensory cortex hind limb region (S1HL), using a micro-drill (110-4103, CircuitMedic, MA, USA). This hole was used to inject virus into the brain. Injections were carried out via a

glass capillary connected to a wireless nanoinjector (Neurostar, Tuebingen, Germany). To consistently inject into S1HL[22], the capillary was placed above bregma, defining this point as 0 for all axes. Then the capillary was moved using a joystick to the aforementioned drilled hole and lowered to the entry of the hole. The injection site was located at 0.02 mm anterior to bregma and 2 mm from the midline. From here the capillary was lowered 1.4 mm into the brain at a rate of 0.2 mm/s. Once at the required depth, the capillary was retracted 100 µm to an injection depth of 1.3 mm. Injection of the virus was carried out at this location (S1HL region) at a rate of 2.5 nL/s. Five minutes after the injection was completed the capillary was retracted from the brain. The hole in the brain was sealed using adhesive luting cement (S380, Parkell Inc., NY, USA). The scalp was closed via suturing and tissue glue (Histoacryl®, Braun, Germany). For all experiments, the physiologic status of the mice including heart rate, body temperature and blood oxygenation were constantly monitored using the PhysioSuite® physiological monitor (Kent Scientific, Torrington, CT, USA). A rectal thermometer and a feedback-controlled heating pad were used to ensure the body temperature of the mice were constant and at a physiological condition (PhysioSuite®, Kent Scientific, Torrington, CT, USA). During surgical procedures anesthesia was maintained using isoflurane at a concentration of 1.0% to 1.5% v/v in 100% O_2 with a flow rate of approximately 0.7 L/min. After the surgery mice were closely monitored for signs of pain and when needed were treated with another drop of Metamizole. All mice removed stitches themselves once the tissue glue had dissolved after 3 days.

Electrical Hindpaw Stimulation. Stainless steel needle electrodes were connected to the mouse paw by carefully inserting them under the skin of the foot pad. The electrodes were connected to a World Precision Instruments Stimulus Isolator (A365, World Precision Instruments, FL, USA). In all cases the applied voltage was set to 0.5 mA. The entire experiment was started via an external trigger that ensured the synchronization of the image acquisition and the paw stimulus. The outputs of the paw stimulus generator were connected to the electrodes in the paw of the mouse via a BNC cable. For single paw stimuli, a 50 ms electrical pulse was applied once every 25 s, at t = 5 s. For stimulation trains 10 pulses with a 20 ms on and 50 ms off duration were applied every 25 s, at t = 5 s. For both paradigms this allowed the first 5 s of the cycle to be used for baseline activity determination. In both cases the stimulation paradigm was repeated every 25 seconds (1 cycle) for a total of 20 cycles. The fluorescence recording was synchronized with the paw stimulation via the initial trigger. Anesthesia levels were kept at 1-1.2% isoflurane v/v in

100% O_2 during paw stimulation experiments, head fixation and monitoring were the same as above.

Imaging. NIR-GECO1 transfected mice were imaged at 10 and 12 days post-injection, while miRFP and PBS injected mice were imaged 14 days post-injection. For virally induced fluorescence, the expression was consistent until ~21 days post injection at which point the fluorescence began to subside. This may be due to increased thickening of the skull and/or skin due to the aging of the mice. The same anesthesia method, head fixation and monitoring was used as outlined above for *in vivo* mesoscale AAV injections. Fluorescent illumination was achieved using a continuous wave 671 nm laser (FPYL-671-50T, Frankfurt Laser Company, Germany) coupled into a multimode fiber bundle (CeramOptec, Germany). The output at the distal end of the fiber was measured to be 41 mW (82% coupling efficiency) and was held in place at an angle of 45° at a distance of 8 cm from the head of the mouse. This setup ensured the entire head of the mouse was evenly illuminated. Fluorescence of NIR-GECO1 was detected by a sCMOS camera (Luca$^{EM®}$, Andor Technology Ltd., UK) at a rate of 5 Hz. Light was collected through a macro lens (Micro-NIKKOR 105 mm, Nikon, Japan) and filtered using an 700 nm Long Pass (Andover, NH, USA) and 721/42 nm Band pass (Andover, NH, USA) held in place using a filter wheel (LTFW6, Thorlabs, NJ, USA). GCaMP6s mice (C57BL/6J-Tg(Thy1-GCaMP6s)GP4.12 (Ref. 3), Stock no. 025776, The Jackson Laboratory, ME, USA) were imaged at 90 and 93 days old in the exact same manner as above aside from laser and filter changes. Prior to imaging and where applicable, the fur above the scalp was removed by firstly shaving the area and then applying hair removal cream (Veet Sensitive Skin Hair Removal Cream, Reckitt Benckiser, Heidelberg, Germany). Application time was approximately 2 minutes per area and all remaining fur was carefully removed using cotton swabs and water. Both the skin and skull remained intact during imaging and were not damaged during the process. Fluorescence excitation was provided by a continuous wave laser at 473 nm (FPYL-473-50T, Frankfurt Laser Company, Germany) coupled into the same fiber with an output of 43 mW at the distal end. In this case a 525/39 nm band pass filter was used to collect emitted light (BrightLine Basic^{TM} Fluorescence Filter, Semrock, NY, USA).

Data Analysis. All data sets were analyzed using custom code in Matlab (Matlab 2017b, Mathworks, MA, USA). The entire recording was imported into Matlab and concatenated into a single matrix. A cycle is defined as a 25 s time period within which a stimulation of the paw

occurs. For all stimulation paradigms of the 20 stimulation cycles the first was removed and the remaining 19 were averaged into a single cycle. Background subtraction was then carried out across the cycle from a 50×50 pixel region of interest (ROI) outside the fluorescent area. The images were smoothed using the imfilter function in Matlab with a kernel size of 25. Due to the photobleaching of the protein the entire cycle was detrended using linear detrending on a pixel by pixel basis. Next, $\Delta F/F_0$ values were determined by dividing the entire cycle by the baseline activity which was defined from a 50×50 pixel region of interest (ROI) from the first 5 seconds of the cycle. The cycle was multiplied by 100 to get the change values in %. The response of the protein across the averaged cycle was calculated from an averaged 50×50 pixel ROI within the fluorescent area. A low pass filter was applied to all traces. For *in vivo* mesoscale activation figures and videos, manual segmentation was applied to highlight the injected brain hemisphere.

Supplementary Note 5: Number of times experiments were repeated independently with similar results.

Fig. 1c: Representative of $n > 3$ independent experiments.

Fig. 1d: Representative of $n > 3$ independent experiments.

Fig. 2a: Representative of $n = 4$ slices from 2 mice.

Fig. 2c: Representative of $n = 129$ neurons from 1 slice from 1 mouse.

Fig. 2f: Mean response data from a single mouse as shown in **Fig. 2e**. Representative of $n = 3$ mice (independent repeats).

Fig. 2g: Mean response data from a single mouse as shown in **Fig. 2e**. Representative of $n = 3$ mice (independent repeats).

Fig. 3a: . Representative of $n > 3$ independent experiments for 1-photon spectra (identical to **Fig. 1c**). $n = 2$ independent experiments for 2-photon spectra.

Fig. 3b: Representative of $n = 2$ cultures.

Fig. 3c: Representative of $n = 32$ neurons from 2 cultures.

Fig. 3d: Representative of $n > 3$ independent experiments (identical to **Fig. 1c**).

Fig. 3e: Representative of $n = 9$ slices from 2 mice.

Fig. 3f: Representative of $n = 9$ slices from 2 mice.

Fig. 3g: Data is representative of 11 cells from 8 independent experiments with similar results. Four additional examples are provided in **Supplementary Fig. 14**.

Fig. 3h: Data is representative of $n = 2$ independent cultures.

Fig. 3i: Representative of $n = 271$, 178, 331 neurons for GCaMP6f, RCaMP1.07, NIR-GECO1, respectively, from 2 cultures.

Supplementary Fig. 5d: Repeated independently more than 3 times with similar results.

Supplementary Fig. 6b: Data is the mean value of $n = 5$ replicates from one experiment.

Supplementary Fig. 7a: Representative of $n = 39$ neurons for NIR-GECO1+BV and $n = 51$ neurons for NIR-GECO1.

Supplementary Fig. 7c: Representative of $n = 15$ neurons for both NIR-GECO1 and NIR-GECO1-T2A-HO1.

Supplementary Fig. 8a: Repeated independently 55 times with similar results (see **Fig. 1i-l**).

Supplementary Fig. 8b: Representative of $n = 4$ slices from 2 mice.

Supplementary Fig. 8c: Data is Representative of $n = 6$ neurons from 4 mice.

Supplementary Fig. 9e: Representative of $n = 5$ neurons from 2 cultures.

Supplementary Fig. 9f: Representative of $n = 5$ neurons from 2 cultures.

Supplementary Fig. 10a: Single image representative of $n = 3$ PBS injected mice (2 injected on the RHS and 1 injected on the LHS) or $n = 3$ mice expressing NIR-GECO1 (1 injected on the RHS and 2 injected on the LHS).

Supplementary Fig. 10c: Mean response data from a single mouse as shown in **Fig. 10b**. Representative of $n = 3$ mice (independent repeats).

Supplementary Fig. 10d: Mean response data from a single mouse as shown in **Fig. 10b**. Representative of $n = 3$ mice (independent repeats).

Supplementary Fig. 11a: Single images representative of $n = 3$ PBS injected mice, $n = 3$ mice expressing NIR-GECO1, $n = 3$ mice expressing GCaMP6s, $n = 3$ mice expressing miRFP and $n = 8$ FoxN1 nude mice under LED illumination (same mice as used for viral or PBS injections).

Supplementary Fig. 11b: Mean response data from $n = 3$ NIR-GECO1 expressing mice (shown in **Fig. 2e**) and $n = 3$ GCaMP6s mice (independent repeats).

Supplementary Fig. 11c: Mean response data from $n = 3$ NIR-GECO1 expressing mice (shown in **Supplementary Fig. 10b**) and $n = 3$ GCaMP6s mice (independent repeats).

Supplementary Fig. 12b: Representative of $n = 184$, 106, and 77 cells, respectively, from one culture.

Supplementary Fig. 12c: Representative of $n = 4$ neurons from 2 cultures.

Supplementary Fig. 12d: *n* = 184, 106, and 77 cells, respectively, from one culture.

Supplementary Fig. 12e: Representative of *n* = 2 slices from one mouse.

Supplementary Fig. 12f: Representative of *n* = 3 field of view from 1 mouse.

Supplementary Fig. 13a: Representative of *n* = 45 and 93 neurons for NIR-GECO1 and NIR-GECO1 + CoChR-EGFP, respectively, from two cultures.

Supplementary Fig. 13b: Representative of *n* = 45 and 93 neurons for NIR-GECO1 and NIR-GECO1 + CoChR-EGFP, respectively, from two cultures.

Supplementary Fig. 13d-e: Repeated more than 10 times with similar results.

Supplementary Fig. 14a-d: Data is representative of 11 cells from 8 independent experiments with similar results. One additional example is provided in **Fig. 3g**.

Supplementary Videos 1: Mean response data from a single mouse as shown in **Fig. 2e**. Representative of *n* = 3 mice (independent repeats).

Supplementary Video 2: Mean response data from a single mouse as shown in **Supplementary Fig. 10b**. Representative of *n* = 3 mice (independent repeats).

Supplementary Video 3: Data is representative of 11 cells from 8 independent experiments with similar results.

Supplementary Video 4: Data is representative of *n* = 271, 178, 331 neurons for GCaMP6f, RCaMP1.07, NIR-GECO1, respectively from 2 cultures.

Supplementary References

1. Piatkevich, K.D. et al. *Nat. Chem. Biol.* **14**, 352-360 (2018).
2. Nakai, J., Ohkura, M. & Imoto, K. *Nat. Biotechnol.* **19**, 137–141 (2001).
3. Chen, T.-W.W. et al. *Nature* **499**, 295–300 (2013).
4. Akerboom, J. et al. *J. Neurosci.* **32**, 13819–13840 (2012).
5. Baird, G.S., Zacharias, D.A. & Tsien, R.Y. *Proc. Natl. Acad. Sci. U. S. A.* **96**, 11241–11246 (1999).
6. Nagai, T., Sawano, A., Park, E.S. & Miyawaki, A. *Proc. Natl. Acad. Sci. U. S. A.* **98**, 3197–3202 (2001).
7. Barykina, N.V. et al. *Sci. Rep.* **6**, 34447 (2016).
8. Zhao, Y. et al. *Science* **333**, 1888–1891 (2011).
9. Akerboom, J. et al. *Front. Mol. Neurosci.* **6**, 2 (2013).
10. Shen, Y. et al. *BMC Biol.* **16**, 9 (2018).
11. Ohkura, M., Sasaki, T., Kobayashi, C., Ikegaya, Y. & Nakai, J. *PLoS One* **7**, e39933 (2012).
12. Wu, J. et al. *ACS Chem. Neurosci.* **4**, 963–972 (2013).
13. Inoue, M. et al. *Nat. Methods* **12**, 64–70 (2014).
14. Wu, J. et al. *Nat. Commun.* **5**, 5262 (2014).
15. Dana, H. et al. *Elife* **5**, e12727 (2016).
16. Wu, J. et al. *ACS Chem. Biol.* **13**, 1832–1837 (2018).
17. Makarov, N.S., Campo, J., Hales, J.M. & Perry, J.W. *Opt. Mater. Express, OME* **1**, 551–563 (2011).
18. Drobizhev, M., Makarov, N.S., Tillo, S.E., Hughes, T.E. & Rebane, A. *Nat. Methods* **8**, 393–399 (2011).
19. Lakowicz, J. R. *Principles of Fluorescence Spectroscopy* 3rd edn (Springer, Berlin, 2006).
20. Piatkevich, K.D. et al. *Biophys. J.* **113**, 2299–2309 (2017).
21. Gottschalk, S., Fehm, T.F., Deán-Ben, X.L. & Razansky, D. *J. Cereb. Blood Flow Metab.* **35**, 531–535 (2015).
22. Franklin, K.B. & Paxinos, G. The mouse brain in stereotaxic coordinates, compact. The coronal plates and diagrams 3rd edition (Amsterdam: Elsevier Academic Press: 2008).